9. Cheson BD, Horning SJ, Coiffier B, et al. Report of an international workshop to standardize response criteria for non-Hodgkin's lymphomas. NCI Sponsored International Working Group. J Clin Oncol 1999;17:1244.
10. Przepiorka D, Weisdorf D, Martin P, et al. 1994 Consensus Conference on Acute GVHD Grading. Bone Marrow Transplant 1995;15:825–828.
11. Shulman HM, Sullivan KM, Weiden PL, et al. Chronic graft-versus-host syndrome in man. A long-term clinicopathologic study of 20 Seattle patients. Am J Med 1980;69:204–217.
12. Gray R. A class of K-sample tests for comparing the cumulative incidence of a competing risk. Ann Stat 1988;16:1140–1154.
13. Fine J, Gray R. A proportional hazards model for the subdistribution of a competing risk. J Am Stat Assoc 1999;15:496–509.
14. Al-Tourah AJ, Gill KK, Chhanabhai M, et al. Population-based analysis of incidence and outcome of transformed non-Hodgkin's lymphoma. J Clin Oncol 2008;26:5165–5169.
15. Rezvani AR, Norasetthada L, Gooley T, et al. Non-myeloablative allogeneic haematopoietic cell transplantation for relapsed diffuse large B-cell lymphoma: A multicentre experience. Br J Haematol 2008;143:395–403.
16. Sirvent A, Dhedin N, Michallet M, et al. Low nonrelapse mortality and prolonged long-term survival after reduced-intensity allogeneic stem cell transplantation for relapsed or refractory diffuse large B cell lymphoma: Report of the Societe Francaise de Greffe de Moelle et de Therapie Cellulaire. Biol Blood Marrow Transplant 2010;16:78–85.
17. Thomson KJ, Morris EC, Bloor A, et al. Favorable long-term survival after reduced-intensity allogeneic transplantation for multiple-relapse aggressive non-Hodgkin's lymphoma. J Clin Oncol 2009;27:426–432.
18. Kim SW, Tanimoto TE, Hirabayashi N, et al. Myeloablative allogeneic hematopoietic stem cell transplantation for non-Hodgkin lymphoma: A nationwide survey in Japan. Blood 2006;108:382–389.
19. Rezvani AR, Storer B, Maris M, et al. Nonmyeloablative allogeneic hematopoietic cell transplantation in relapsed, refractory, and transformed indolent non-Hodgkin's lymphoma. J Clin Oncol 2008;26:211–217.
20. Doocey RT, Toze CL, Connors JM, et al. Allogeneic haematopoietic stem-cell transplantation for relapsed and refractory aggressive histology non-Hodgkin lymphoma. Br J Haematol 2005;131:223–230.
21. Ramadan KM, Song KW, Connors JM, et al. Comparison of outcome between refractory/relapsed de novo diffuse large B-cell and transformed lymphoma using related and unrelated allogeneic hematopoietic SCT. Blood 2008;112: abstract no. 2173.
22. Ramadan KM, Connors JM, Al-Tourah A, et al. Salvage therapy with allogeneic stem cell transplantation results in better outcome for patients with relapsed-refractory follicular lymphoma compared to those with transformed non-Hodgkin lymphoma: A population-based comparative study. Blood 2008;112: abstract no. 975.
23. Kuruvilla J, Pond G, Tsang R, et al. Favorable overall survival with fully myeloablative allogeneic stem cell transplantation for follicular lymphoma. Biol Blood Marrow Transplant 2008;14:775–782.
24. Khouri IF, McLaughlin P, Saliba RM, et al. Eight-year experience with allogeneic stem cell transplantation for relapsed follicular lymphoma after nonmyeloablative conditioning with fludarabine, cyclophosphamide, and rituximab. Blood 2008;111:5530–5536.
25. Oliansky DM, Gordon LI, King J, et al. The role of cytotoxic therapy with hematopoietic stem cell transplantation in the treatment of follicular lymphoma: An evidence-based review. Biol Blood Marrow Transplant 2010;16:443–468.
26. Gisselbrecht C, Glass B, Mounier N, et al. Salvage regimens with autologous transplantation for relapsed large B-cell lymphoma in the rituximab era. J Clin Oncol 2010;28:4184–4190.
27. Fenske TS, Hari PN, Carreras J, et al. Impact of pre-transplant rituximab on survival after autologous hematopoietic stem cell transplantation for diffuse large B cell lymphoma. Biol Blood Marrow Transplant 2009;15:1455–1464.
28. Hoerr AL, Gao F, Hidalgo J, et al. Effects of pretransplantation treatment with rituximab on outcomes of autologous stem-cell transplantation for non-Hodgkin's lymphoma. J Clin Oncol 2004;22:4561–4566.
29. Alizadeh AA, Eisen MB, Davis RE, et al. Distinct types of diffuse large B-cell lymphoma identified by gene expression profiling. Nature 2000;403:503–511.
30. Davies AJ, Rosenwald A, Wright G, et al. Transformation of follicular lymphoma to diffuse large B-cell lymphoma proceeds by distinct oncogenic mechanisms. Br J Haematol 2007;136:286–293.
31. Maeshima AM, Omatsu M, Nomoto J, et al. Diffuse large B-cell lymphoma after transformation from low-grade follicular lymphoma: morphological, immunohistochemical, and FISH analyses. Cancer Sci 2008;99:1760–1768.

Bone Marrow Transplantation (2013) **48,** 74–79

www.nature.com/bmt

ORIGINAL ARTICLE

Stenotrophomonas maltophilia infection in hematopoietic SCT recipients: high mortality due to pulmonary hemorrhage

K Tada[1], S Kurosawa[1], N Hiramoto[1], K Okinaka[1], N Ueno[1], Y Asakura[1], S-W Kim[1], T Yamashita[1], S-I Mori[1], Y Heike[1], AM Maeshima[2], R Tanosaki[2], K Tobinai[1] and T Fukuda[1]

To clarify the clinical features and outcome of *Stenotrophomonas maltophilia* infection among hematopoietic SCT (HCT) recipients, we retrospectively reviewed the records of 1085 consecutive HCT recipients and identified 42 episodes in 31 HCT recipients with *S. maltophilia* infection. We compared these recipients with 30 non-HCT patients with *S. maltophilia* infection. The mortality rate in HCT recipients was significantly higher than that in non-HCT patients (relative risk 5.7, $P=0.04$), and we identified seven patients with pulmonary hemorrhage due to *S. maltophilia*, exclusively in the HCT cohort. Six of these latter seven patients died within 1 day from the onset of hemorrhage and the isolate was identified after death in most cases; one patient, who received empiric therapy for *S. maltophilia* and granulocyte transfusion, survived for more than 2 weeks. The patients with pulmonary hemorrhage had a more severe and longer duration of neutropenia, persistent fever despite of the use of broad-spectrum antibiotics, complication by pneumonia and higher C-reactive protein levels than those without pulmonary hemorrhage. In conclusion, *S. maltophilia* was associated with fulminant and fatal pulmonary hemorrhage in HCT recipients. Empiric therapy with antibiotics before the onset of pulmonary hemorrhage may be effective in HCT recipients who carry the conditions identified.

Bone Marrow Transplantation (2013) **48,** 74–79; doi:10.1038/bmt.2012.87; published online 28 May 2012

Keywords: *Stenotrophomonas maltophilia*; SCT; pulmonary hemorrhage

INTRODUCTION

Stenotrophomonas maltophilia is a non-fermentative, Gram-negative bacillus that is ubiquitous in the natural and hospital environment,[1–4] and exhibits intrinsic resistance to many antibiotics including β-lactams, carbapenems and aminoglycosides.[5,6] Although *S. maltophilia* is not usually highly virulent, it is a significant pathogen in immune-compromised patients, and the incidence of *S. maltophilia* infection is increasing.[7]

Previously, in a heterogeneous group that included recipients of hematopoietic SCT (HCT) and non-HCT patients with solid tumor or hematological malignancy, risk factors for acquiring *S. maltophilia* infection were reported to be prolonged neutropenia, exposure to broad-spectrum antibiotics, mucositis, indwelling medical devices such as an intravascular catheter or ventilation tubes and long hospital stays.[8–12] In a similarly heterogeneous group, risk factors for mortality of *S. maltophilia* infection were reported to be neutropenia, hematological malignancy, immunosuppressive therapy, shock status at infection onset and intensive-care unit stays.[13–17] However, only limited information is available on HCT recipients.[12,18,19] Many of the previously reported risk factors are commonly seen in HCT recipients because of their severe immunosuppressive status and mucositis due to preparative conditioning and immunosuppressive therapy for GVHD prophylaxis.

Hence, *S. maltophilia* infection in HCT recipients may have a different spectrum and greater severity compared with that in patients with solid tumor or non-HCT setting hematological malignancy. To clarify the clinical features and outcome of *S. maltophilia* infection with a particular focus on HCT recipients, we retrospectively analyzed clinical data on patients who had *S. maltophilia* infection.

PATIENTS AND METHODS

Patients

We retrospectively reviewed the medical and microbiological records of all the HCT recipients at the National Cancer Center Hospital (Tokyo, Japan) between January 2001 and December 2010, and identified episodes of *S. maltophilia* blood stream infection (BSI) among the HCT recipients. We also reviewed the medical and microbiological records of all patients whose blood cultures were positive for *S. maltophilia* at our institution in the same period and identified episodes of *S. maltophilia* BSI among the non-HCT patients. We then compared the clinical features and outcomes in the HCT cohort with those in the non-HCT control cohort.

Definitions

An episode of *S. maltophilia* BSI was defined as one or more positive blood cultures for *S. maltophilia* with clinical signs of infection. When *S. maltophilia* was again detected in the same patient at an interval of 8 or more days after the first BSI episode had improved, the detection of the isolate was regarded as a different episode of BSI, as previously reported.[13,20] The severity of illness was assessed by the bacteremia score according to the University of Pittsburgh (PITT score).[21,22] The D-index and cumulative D-index, which were calculated as the area over the neutrophil curve that is based on a graph plotting the absolute neutrophil counts during neutropenia,[23] were also investigated to evaluate the impact of both duration and severity of neutropenia on *S. maltophilia* infection.

Infection control in HCT recipients and microbiological investigations

Among the HCT recipients, prophylaxis for infection consisted of trimethoprim-sulfamethoxazole (ST), ciprofloxacin, fluconazole and acyclovir. As therapy for febrile neutropenia, cefepim was first administered in

[1]Department of Hematology and Hematopoietic Stem Cell Transplantation, National Cancer Center Hospital, Tokyo, Japan and [2]Department of Pathology and Clinical Laboratories, National Cancer Center Hospital, Tokyo, Japan. Correspondence: Dr T Fukuda, Department of Hematology and Hematopoietic Stem Cell Transplantation, National Cancer Center Hospital, 5-1-1 Tsukiji, Chuo-ku, Tokyo 104-0045, Japan.
E-mail: tafukuda@ncc.go.jp
Received 29 December 2011; revised 3 April 2012; accepted 9 April 2012; published online 28 May 2012

most cases, and in cases that did not improve within 2–3 days, either it was switched to carbapenem or vancomycin was added.

Two sets of blood culture samples from a double-lumen intravascular catheter and another from peripheral blood were routinely taken at the initial episode of fever. If fever persisted, one set of the blood culture samples was taken daily from either the lumen of the intravascular catheter or a peripheral vessel alternately. Blood culture samples were processed using a BACTEC 9240 (before 2008) or BACTEC FX (after 2009) system (Becton Dickinson Microbiology Systems, Sparks, MD, USA). Susceptibility to antibiotics was tested by the broth microdilution method according to the guidelines of the National Committee for Clinical Laboratory Standards.

Statistical analysis

The end point was defined as death within 4 weeks from the onset of a positive blood culture for *S. maltophilia*. Categorical variables were analyzed using a Chi-squared test or Fisher's exact test as appropriate. Continuous variables were compared using the Mann–Whitney *U*-test. To investigate risk factors for death within 4 weeks in all cases including both HCT and non-HCT cases, a multivariate logistic regression analysis was performed. The following factors were used as covariates: age (<45 vs $\geqslant 45$ y), severe neutropenia at BSI onset, PITT score ($\leqslant 1$ vs >1), complication by pneumonia and therapy for underlying disease (HCT vs non-HCT). The statistical analysis was performed with the SPSS 11.0 statistical software package (SPSS Inc, Tokyo, Japan).

RESULTS

Patient characteristics

In the study period between 2001 and 2010, a total of 1085 HCT (847 allogeneic HCT and 238 autologous HCT) procedures were performed in our institution. A total of 42 episodes (35 episodes in allogeneic HCT recipients and 7 episodes in autologous HCT recipients) of *S. maltophilia* BSI were identified in 31 HCT recipients (2.9%). There was no obvious outbreak of *S. maltophilia* infection in the study period.

The patient characteristics are shown in Table 1. Broad-spectrum cefem or carbapenem was administered in 60% of the episodes at BSI onset. With regard to the therapy for *S. maltophilia* infection, the intravascular catheter was removed in 10 (24%) episodes in which catheter-related BSI was suspected. When *S. maltophilia* BSI was diagnosed, ST or fluoroquinolone was started based on the susceptibility test in 19 episodes, whereas no antibiotics were additionally administered in 7 episodes where *S. maltophilia* was only detected in blood culture after death.

Clinical outcome

In all, 14 patients died within 4 weeks from the onset of a positive blood culture for *S. maltophilia*. We divided causes of death into two patterns; eight patients were judged to have died from a single cause due to *S. maltophilia* infection, whereas six appeared to have died of complex causes, which consisted of *S. maltophilia* infection and some other cause (underlying disease progression in two, GVHD in two, other infection in one and suffocation due to vomiting in one). Pulmonary hemorrhage accounted for half of the 14 deaths. Among the 847 allogeneic HCT recipients, 18 patients (2.1%) developed pulmonary hemorrhage (infection of *S. maltophilia*: $n=7$, Aspergillus species: $n=3$, *Pseudomonas aeruginosa*: $n=1$, Staphylococcus species: $n=1$, cytomegalovirus: $n=1$, idiopathic pneumonia syndrome/diffuse alveolar hemorrhage: $n=2$, disseminated intravascular coagulation: $n=1$, tumor invasion: $n=1$ and unknown cause: $n=1$).

Seven cases with pulmonary hemorrhage

The details of the seven patients with pulmonary hemorrhage are shown in Table 2. All the episodes of pulmonary hemorrhage occurred during a period of profound neutropenia (neutrophil count 0/μL).

Table 1. Patients and clinical characteristics of HCT recipients who developed *S. maltophilia* BSI

	Total 31 patients (42 episodes)	%
Age, median, range	44 years, 4–67 (43 years, 4–67)	
Sex (male/female)	25/6 (34/7)	81/19 (81/19)
Underlying disease		
Leukemia	19 (24)	61 (57)
Lymphoma	7 (9)	23 (21)
MDS/myelofibrosis	3 (3)	10 (7)
Solid tumor	2 (6)	6 (14)
Type of HCT		
Allogeneic	28 (35)	90 (83)
Autologous	3 (7)	10 (17)
Conditioning for allo-HCT		
Myeloablative	15 (19)	54 (54)
Reduced intensity	13 (16)	46 (46)
Donor and source		
Related PB	8 (9)	26 (21)
Related BM	1 (1)	3 (2)
Unrelated BM	14 (18)	45 (43)
Cord blood	5 (7)	16 (17)
Autologous PB	3 (7)	10 (17)
Immunosuppressive agents		
CSP ± steroid	13 (16)	42 (38)
TAC ± steroid	9 (11)	29 (26)
Steroid	4 (4)	13 (10)
None	5 (11)	16 (26)
CV indwelling	30 (41)	97 (98)
Antibiotics at BSI onset		
Carbapenem ± vancomycin	13 (18)	42 (43)
Broad cefem or penicillin	6 (7)	19 (17)
Ciprofloxacin (prophylaxis)	8 (9)	26 (21)
ST (prophylaxis)	2 (4)	6 (10)
Other	1 (1)	3 (2)
None	1 (3)	1 (7)
Therapy for infection		
CV removal	7 (10)	23 (24)
Granulocyte Transfusion	2 (2)	6 (5)
ST	5 (5)	16 (12)
ST + quinolone	3 (3)	10 (7)
ST + ceftazidime	1 (2)	3 (5)
Quinolone ± minocyclin	7 (9)	23 (21)
Ceftazidime	3 (4)	10 (7)
None	9 (9)	29 (21)

Abbreviations: BSI = blood stream infection; CSP = cyclosporine; CV = central venous catheter; HCT = hematopoietic SCT; MDS = myelodysplastic syndrome; PB = peripheral blood; ST = trimethoprim-sulfamethoxazole; TAC = tacrolimus.

As initial symptoms, all patients showed persistent fever that did not respond to broad-spectrum antibiotics. Other symptoms included chest pain ($n=4$), back pain ($n=2$), hemosputum ($n=2$) or dyspnea ($n=1$). Imaging test findings of chest X-ray ($n=5$) or computed tomography ($n=5$) in all patients showed consolidation that was consistent with symptoms such as chest pain. Six patients (cases 1–3 and 5–7) developed massive hemoptysis within 1–4 days after the initial chest symptoms. At the onset of massive hemoptysis, all the patients developed respiratory and circulatory failure due to bleeding and sepsis. Six patients, but not case 7, died within 1 day after hemoptysis.

Table 2. Details of patients with pulmonary hemorrhage due to *S. maltophilia*

Case	Age/ gender	Underlying disease	Type of HCT	Conditioning	Onset day[a] of hemorrhage	Day[a] of death	Day[a] of identification of S maltophilia		Treatment for S maltophilia infection
							Sputum	Blood	
1	27/M	AML	CBT	CA + CY + TBI 12 Gy	10	10	After death	After death	None
2	37/M	Myelofibrosis	U-BMT	BU + CY	11	11	After death	After death	None
3	54/M	AML	U-BMT	CY + TBI 12 Gy	15	16	12	After death	None
4	58/M	AML	CBT (second allogeneic HCT)	Flu + BU + TBI 2 Gy	18	18	9	After death	CAZ
5	43/M	AML	CBT (second allogeneic HCT)	Flu + Mel	6	7	Previously known	After death	ST + PZFX + CAZ
6	24/M	AML	R-PBSCT	BU + CY	445 (11)[b]	446 (12)[b]	NA	445 (11)[b]	ST
7	51/M	AML	U-BMT	BU + CY	39	55	42	40	ST + PZFX granulocyte transfusion

Abbreviations: CA = cytarabine; CAZ = ceftazidime; CBT = cord blood transplantation; Flu = fludarabine; HCT = hematopoietic SCT; Mel = melpharan; NA = not assessment; PZFX = pazufloxacin; R-PBSCT = related PBSCT; ST = trimethoprim-sulfamethoxazole; U-BMT = unrelated BMT. [a]Day after allogeneic HCT. [b]Day after chemotherapy using idarubicin and cytarabine for relapse after allogeneic HCT.

Because of the significantly rapid clinical course, *S. maltophilia* was detected in blood culture after death or 1 day before death in six patients (cases 1–6) and, similarly, *S. maltophilia* was detected in sputum culture after death in two patients (case 1 and 2).

Therapy for *S. maltophilia* was not initiated in three cases (cases 1–3) because the isolate was identified after death. In case 7, the administration of ST and pazufloxacin was started before the onset of hemoptysis and the identification of isolate because pulmonary hemorrhage due to *S. maltophilia* was suspected based on a typical clinical course and imaging test findings. Granulocyte transfusion was also started 38 h after the onset of hemoptysis and 28 h after the detection of *S. maltophilia* in blood culture. This patient survived for 16 and 15 days after the onset of hemoptysis and the identification of BSI, respectively. However, he eventually died due to *S. maltophilia* infection associated with primary graft failure. In case 5, the administration of ST and pazufloxacin was started before hemoptysis because he had a past history of *S. maltophilia* infection. The isolates exhibited resistance to the antibiotics used and he died within 1 day after hemoptysis. Bronchial arterial embolization was performed for pulmonary hemorrhage in two patients (case 1 and 5), however, neither were rescued.

Pulmonary hemorrhage due to *S. maltophilia* was diagnosed by the detection of *S. maltophilia* in blood and sputum cultures, histopathological findings of pulmonary hemorrhage and the presence of massive infiltration of Gram-negative rods in lungs by autopsy in three cases (cases 2, 3 and 5) (Figure 1). Cases 1 and 7 were diagnosed by the detection of *S. maltophilia* in blood and sputum cultures and the confirmation of pulmonary hemorrhage using bronchoscopy. Case 4 was diagnosed by the detection of *S. maltophilia* in blood and sputum cultures and clinical symptoms such as hemoptysis. Case 6 was diagnosed by the detection of *S. maltophilia* in blood culture and pulmonary hemorrhage confirmed by bronchoscopy.

Although the histopathological findings at autopsy in case 2 demonstrated one focal small nodule of aspergillosis in the right upper lobe, pulmonary hemorrhage was mainly found in the bilateral lower lobes, and therefore was mainly assumed to be due to *S. maltophilia* infection. There was no histopathological evidence of fungal infection in the other autopsy cases. Serum galactomannan Ag and β-D-glucan were tested at around the onset of pulmonary hemorrhage and results were negative in six cases, but not in case 2. The clinical characteristics and outcome in patients with and without pulmonary hemorrhage are compared in Table 3. Patients with pulmonary hemorrhage were associated with severe and longer duration of neutropenia, higher C-reactive protein levels at BSI onset, a higher D- and cumulative D-index, a higher incidence of complication by pneumonia and higher mortality than those without pulmonary hemorrhage.

Comparison of HCT recipients with non-HCT patients

The clinical characteristics and outcomes of HCT recipients (42 episodes) were compared with those of 30 non-HCT patients (15 episodes with hematological malignancy and 15 with solid tumor) who developed *S. maltophilia* infection (Table 3). HCT recipients were more likely to be associated with severe neutropenia (<100/μL), use of immunosuppressive agents and a higher mortality within 4 weeks after *S. maltophilia* BSI than non-HCT patients.

Although there was no significant difference in the proportion of patients with *S. maltophilia* pneumonia between the HCT recipients and non-HCT patients, pulmonary hemorrhage was seen only in HCT recipients. By a multivariate analysis in all the 72 episodes, including both HCT ($n = 42$) and non-HCT cases ($n = 30$), the independent risk factors for mortality within 4 weeks after *S. maltophilia* BSI were HCT recipient (relative risk 5.7, 95% confidence interval 1.1–30.1, $P = 0.04$) and complication by pneumonia (relative risk 10.7, 95% confidence interval 2.6–44.2, $P = 0.001$).

Susceptibility of strains of *S. maltophilia* from HCT recipients

A total of 41 strains of *S. maltophilia* isolated from HCT recipients were tested with regard to their susceptibility to antibiotics. The percentages of isolates that were susceptible to ST (81%), minocycline (93%) and levofloxacin (68%) were relatively high, whereas fewer isolates were susceptible to ceftazidime (26%), amikacin (21%), cefepime (5%) and imipenem (3%). There were no significant differences in susceptibility to each antibiotic between isolates from HCT recipients and those from non-HCT patients.

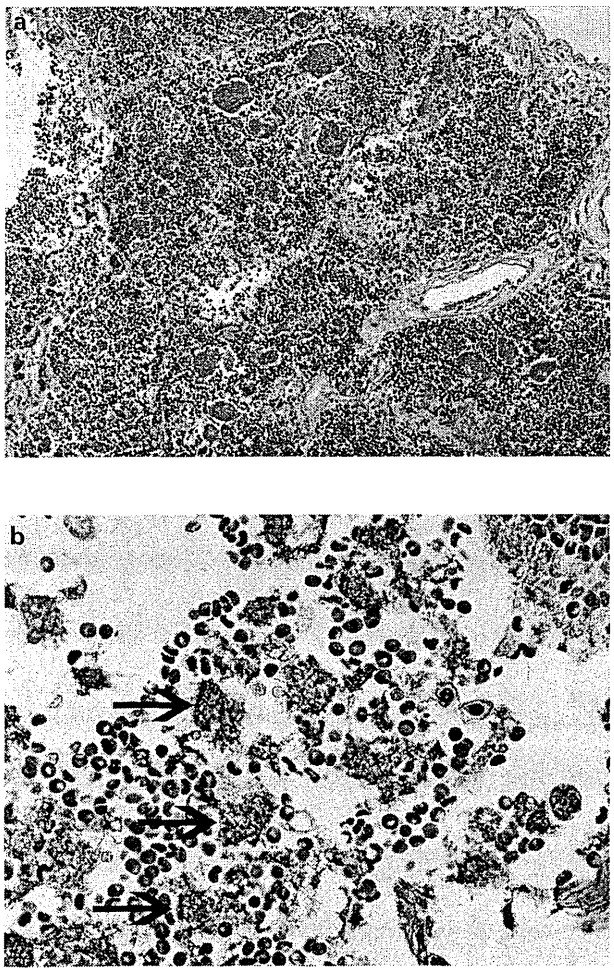

Figure 1. Lung section from case 5 (autopsy). (**a**) Massive intraalveolar hemorrhage and disseminated foci of basophilic bacteria (hematoxylin and eosin stain, ×40). (**b**) Higher magnification of hematoxylin and eosin staining showed a striking number of basophilic bacilli (arrow) without infiltration of the alveoli neutrophils and lymphocytes (×400).

DISCUSSION

This is a retrospective study reporting the clinical characteristics and outcomes of *S. maltophilia* infection with a particular focus on HCT recipients. Our data revealed that HCT recipients who had *S. maltophilia* infection were more likely to be associated with pulmonary hemorrhage, which was the main cause of death in the cohort, and had a higher mortality within 4 weeks after *S. maltophilia* BSI than non-HCT patients.

Previous studies of *S. maltophilia* infection in HCT recipients included many patients with catheter-related BSI and emphasized the removal of an intravascular catheter and the administration of appropriate antibiotics according to the results of a susceptibility test.[13,18,19] Our results were consistent with those of previous studies because 28 out of 42 episodes (67%) of *S. maltophilia* infection in this study were successfully treated. However, in previous reports that included *S. maltophilia* infection in HCT recipients, there was no information on pulmonary hemorrhage due to *S. maltophilia*.[13,18,19] Additionally, in previous large studies of post-transplant pulmonary hemorrhage, *S. maltophilia* had not been detected as a cause of pulmonary hemorrhage.[24–26] There have been only a few reported cases in a non-HCT setting that were associated with pulmonary hemorrhage due to *S. maltophilia* after intensive chemotherapy against hematological malignancy.[27–30] Hence, this is the first report to comprehensively describe the overall picture of pulmonary hemorrhage due to *S. maltophilia* with a particular focus on HCT recipients, including the histopathological findings of autopsy, incidence, typical clinical course, risk factors and outcome.

By reviewing the medical records in detail, we identified the clinical characteristics of post-transplant pulmonary hemorrhage due to *S. maltophilia*. Risk factors for pulmonary hemorrhage due to *S. maltophilia* were HCT recipient, prolonged days of neutropenia, high C-reactive protein level at BSI onset and complication by pneumonia. In addition to the duration of neutropenia, the D- and cumulative D-index[23] were also considered to be factors that predicted pulmonary hemorrhage, whereas a high PITT score at the onset of BSI was not associated with pulmonary hemorrhage.

Typical findings that were recognized before pulmonary hemorrhage were persistent fever despite of the use of broad-spectrum antibiotics, chest symptoms, such as chest pain, and apparent consolidation in imaging test. In many cases, it was impossible to start antibiotic therapy based on the identification of *S. maltophilia* infection in blood or sputum culture because most patients developed a very aggressive clinical course and died before the *S. maltophilia* infection was detected. Hence, *S. maltophilia* infection should be predicted in the HCT recipients based on the presence of risk factors for pulmonary hemorrhage due to *S. maltophilia*, and treatment for *S. maltophilia* infection should be considered before hemoptysis occurs.

In one of our cases (case 7 in Table 2), *S. maltophilia* infection was suspected based on typical findings and risk factors for pulmonary hemorrhage due to *S. maltophilia*, and empiric therapy that consisted of ST and pazufloxacin was started before hemoptysis and the detection of isolate. Granulocyte transfusion was also started, which resulted in a long survival after pulmonary hemorrhage was observed. This case suggests that empiric therapy for *S. maltophilia* infection might be useful if typical findings appear in HCT recipients who have risk factors for pulmonary hemorrhage due to *S. maltophilia*.

Current treatment recommendations for antibiotics against *S. maltophilia* are based on historical evidence, case series, case reports and *in vitro* susceptibility tests because of the lack of controlled trials.[1,6] In general, ST has been shown to have the most potent and reliable *in vitro* activity against *S. maltophilia*, and alternate agents are new fluoroquinolone, tigecycline and ticarcillin–clavulanate. The isolates from both HCT recipients and non-HCT patients in our study were confirmed to have a high *in vitro* susceptibility to ST and new fluoroquinolone, however, tigecycline and ticarcillin–clavulanate were not tested because these drugs have not yet been approved in our country. Hence, ST alone or in combination with other susceptible agents is considered to be the treatment of choice for suspected or culture-proven *S. maltophilia* infection in HCT recipients. However, the myelotoxicity of ST might be a concern in the setting of HCT before engraftment.

The mechanism of *S. maltophilia*-induced pulmonary hemorrhage remains uncertain. *In vitro* data demonstrated that *S. maltophilia* produces proteases, which can break down the protein components of collagen, fibronectin and fibrinogen,[31,32] and this may contribute to local tissue damage and hemorrhage.[1] Because our present histopathological findings at autopsy demonstrated alveolar hemorrhage and the massive infiltration of Gram-negative rods in lungs without invasion by neutrophils or lymphocytes, *S. maltophilia* itself might damage lung tissue, which leads to pulmonary hemorrhage. In an HCT recipient with a highly immunosuppressive background, it is speculated that *S. maltophilia* infects and proliferates in lung tissue, which is fragile due to chemotherapy or TBI as a preparative conditioning, and thus leads to pulmonary hemorrhage with a coexisting tendency for

Table 3. Comparison of clinical characteristics and outcomes

	HCT cohort without pulmonary hemorrhage n = *35 (%)*	*HCT cohort with pulmonary hemorrhage* n = *7 (%)*	P	*HCT cohort* n = *42 (%)*	*Non-HCT cohort* n = *30 (%)*	P
Age, median, range	44, 4–67	43, 24–58	0.7	44, 4–67	49, 4–78	0.1
CRP (mg/dL) at BSI onset, median, range	3.0, 0.2–30.3	25.4, 5–31.2	0.001	4.9, 0.2–31.2	5.3, 0.5–23.4	0.9
Neutropenia (<500/μL) at BSI onset	20 (57)	7 (100)	0.04	27 (64)	13 (43)	0.08
Profound neutropenia (<100/μL) at BSI onset	19 (54)	7 (100)	0.03	26 (62)	10 (33)	0.02
Total days of neutropenia[a], median, range	4, 0–143	25, 6–143	0.02	7, 0–143	0, 0–92	0.09
Total days of profound neutropenia[a], median, range	2, 0–133	12, 4–133	0.02	4, 0–133	0, 0-84	0.05
D-index, median, range	1550, 0-70070	10400, 2600-70070	0.02	2950, 0-70070	0, 0-44400	0.09
Cumulative D-index, median, range	125, 0-46570	8400, 2600-64570	0.006	1550, 0-64570	0, 0-30200	0.08
PITT score >1	3 (9)	7 (100)	0.2	10 (17)	7 (23)	0.8
Coinfection	6 (17)	2 (29)	0.4	8 (19)	5 (17)	0.9
Use of immunosuppressive agents	24 (69)	7 (100)	0.2	31 (74)	2 (7)	<0.001
Pneumonia	10 (29)	7 (100)	0.001	17 (40)	9 (30)	0.4
Pulmonary hemorrhage	–	–	–	7 (17)	0 (0)	0.02
Death within 4 weeks	7 (20)	7 (100)	<0.001	14 (33)	3 (10)	0.02

Abbreviations: BSI = blood stream infection; CRP = C-reactive protein; HCT = hematopoietic SCT. [a]Day from onset of neutropenia (<500/μL) or profound neutropenia (<100/μL) to recovery of neutropenia or profound neutropenia. If a patient died without recovery of neutropenia, days of neutropenia or profound neutropenia were counted until the day of mortality.

bleeding due to a low platelet count and coagulation disorder. Further molecular microbiological studies are warranted to clarify the mechanism of *S. maltophilia*-induced pulmonary hemorrhage.

Our results also showed that most patients who died without pulmonary hemorrhage had complex causes of death, such as underlying disease progression or uncontrolled GVHD in addition to *S. maltophilia* infection. This might be due to the fact that infections due to *S. maltophilia* occur often in patients in poor condition.

Our study has some limitations; it includes a relatively small number of patients in a single institution and uses a retrospective study design. However, this is the largest study to focus on *S. maltophilia* infection in HCT recipients and is the first study to report the significance of pulmonary hemorrhage as a cause of death.

In conclusion, we showed that *S. maltophilia* infection in HCT recipients is associated with higher mortality than that in non-HCT patients, and causes fulminant and fatal pulmonary hemorrhage, which is a main cause of death in HCT recipients with *S. maltophilia* infection. We also showed that patients with pulmonary hemorrhage were associated with persistent fever despite of the use of broad-spectrum antibiotics, complication by pneumonia, severe and significantly longer duration of neutropenia and higher C-reactive protein levels at the onset of BSI than those without pulmonary hemorrhage. Empiric therapy before the onset of pulmonary hemorrhage may be effective in HCT recipients who exhibit these identified conditions because most patients with pulmonary hemorrhage due to *S. maltophilia* die within a short period without the detection of infection. Multicenter prospective or retrospective studies that focus on HCT recipients are warranted to evaluate the optimum therapeutic strategy against this fatal and intrinsic multidrug-resistant microbe.

CONFLICT OF INTEREST

The authors declare no conflict of interest.

REFERENCES

1 Looney WJ, Narita M, Muhlemann K. *Stenotrophomonas maltophilia*: an emerging opportunist human pathogen. *Lancet Infect Dis* 2009; **9**: 312–323.
2 Hoefel D, Monis PT, Grooby WL, Andrews S, Saint CP. Profiling bacterial survival through a water treatment process and subsequent distribution system. *J Appl Microbiol* 2005; **99**: 175–186.
3 Spencer RC. The emergence of epidemic, multiple-antibiotic-resistant *Stenotrophomonas (Xanthomonas) maltophilia* and *Burkholderia (Pseudomonas) cepacia*. *J Hosp Infect* 1995; **30**(Suppl): 453–464.
4 Cervia JS, Ortolano GA, Canonica FP. Hospital tap water as a source of *Stenotrophomonas maltophilia* infection. *Clin Infect Dis* 2008; **46**: 1485–1487.
5 Khardori N, Reuben A, Rosenbaum B, Rolston K, Bodey GP. In vitro susceptibility of *Xanthomonas (Pseudomonas) maltophilia* to newer antimicrobial agents. *Antimicrob Agents Chemother* 1990; **34**: 1609–1610.
6 Nicodemo AC, Paez JI. Antimicrobial therapy for *Stenotrophomonas maltophilia* infections. *Eur J Clin Microbiol Infect Dis* 2007; **26**: 229–237.
7 Safdar A, Rolston KV. *Stenotrophomonas maltophilia*: changing spectrum of a serious bacterial pathogen in patients with cancer. *Clin Infect Dis* 2007; **45**: 1602–1609.
8 Boktour M, Hanna H, Ansari S, Bahna B, Hachem R, Tarrand J *et al.* Central venous catheter and *Stenotrophomonas maltophilia* bacteremia in cancer patients. *Cancer* 2006; **106**: 1967–1973.
9 Metan G, Hayran M, Hascelik G, Uzun O. Which patient is a candidate for empirical therapy against *Stenotrophomonas maltophilia* bacteraemia? An analysis of associated risk factors in a tertiary care hospital. *Scand J Infect Dis* 2006; **38**: 527–531.
10 Trouillet JL, Chastre J, Vuagnat A, Joly-Guillou ML, Combaux D, Dombret MC *et al.* Ventilator-associated pneumonia caused by potentially drug-resistant bacteria. *Am J Respir Crit Care Med* 1998; **157**: 531–539.
11 Martino R, Martinez C, Pericas R, Salazar R, Solá C, Brunet S *et al.* Bacteremia due to glucose non-fermenting gram-negative bacilli in patients with hematological neoplasias and solid tumors. *Eur J Clin Microbiol Infect Dis* 1996; **15**: 610–615.
12 Labarca JA, Leber AL, Kern VL, Territo MC, Brankovic LE, Bruckner DA *et al.* Outbreak of *Stenotrophomonas maltophilia* bacteremia in allogenic bone marrow transplant patients: role of severe neutropenia and mucositis. *Clin Infect Dis* 2000; **30**: 195–197.
13 Araoka H, Baba M, Yoneyama A. Risk factors for mortality among patients with *Stenotrophomonas maltophilia* bacteremia in Tokyo, Japan, 1996-2009. *Eur J Clin Microbiol Infect Dis* 2010; **29**: 605–608.
14 Micozzi A, Venditti M, Monaco M, Friedrich A, Taglietti F, Santilli S *et al.* Bacteremia due to *Stenotrophomonas maltophilia* in patients with hematologic malignancies. *Clin Infect Dis* 2000; **31**: 705–711.

15 Muder RR, Harris AP, Muller S, Edmond M, Chow JW, Papadakis K *et al.* Bacteremia due to Stenotrophomonas (Xanthomonas) maltophilia: a prospective, multicenter study of 91 episodes. *Clin Infect Dis* 1996; **22**: 508–512.
16 Paez JI, Tengan FM, Barone AA, Levin AS, Costa SF. Factors associated with mortality in patients with bloodstream infection and pneumonia due to *Stenotrophomonas maltophilia*. *Eur J Clin Microbiol Infect Dis* 2008; **27**: 901–906.
17 Paez JI, Costa SF. Risk factors associated with mortality of infections caused by *Stenotrophomonas maltophilia*: a systematic review. *J Hosp Infect* 2008; **70**: 101–108.
18 Chaplow R, Palmer B, Heyderman R, Moppett J, Marks DI. *Stenotrophomonas maltophilia* bacteraemia in 40 haematology patients: risk factors, therapy and outcome. *Bone Marrow Transplant* 2010; **45**: 1109–1110.
19 Yeshurun M, Gafter-Gvili A, Thaler M, Keller N, Nagler A, Shimoni A. Clinical characteristics of *Stenotrophomonas maltophilia* infection in hematopoietic stem cell transplantation recipients: a single center experience. *Infection* 2010; **38**: 211–215.
20 Friedman ND, Korman TM, Fairley CK, Franklin JC, Spelman DW. Bacteraemia due to *Stenotrophomonas maltophilia*: an analysis of 45 episodes. *J Infect* 2002; **45**: 47–53.
21 Korvick JA, Bryan CS, Farber B, Beam Jr TR, Schenfeld L, Muder RR *et al.* Prospective observational study of Klebsiella bacteremia in 230 patients: outcome for antibiotic combinations versus monotherapy. *Antimicrob Agents Chemother* 1992; **36**: 2639–2644.
22 Chow JW, Yu VL. Combination antibiotic therapy versus monotherapy for gram-negative bacteraemia: a commentary. *Int J Antimicrob Agents* 1999; **11**: 7–12.
23 Portugal RD, Garnica M, Nucci M. Index to predict invasive mold infection in high-risk neutropenic patients based on the area over the neutrophil curve. *J Clin Oncol* 2009; **27**: 3849–3854.
24 Majhail NS, Parks K, Defor TE, Weisdorf DJ. Diffuse alveolar hemorrhage and infection-associated alveolar hemorrhage following hematopoietic stem cell transplantation: related and high-risk clinical syndromes. *Biol Blood Marrow Transplant* 2006; **12**: 1038–1046.
25 Wanko SO, Broadwater G, Folz RJ, Chao NJ. Diffuse alveolar hemorrhage: retrospective review of clinical outcome in allogeneic transplant recipients treated with aminocaproic acid. *Biol Blood Marrow Transplant* 2006; **12**: 949–953.
26 Gupta S, Jain A, Warneke CL, Gupta A, Shannon VR, Morice RC *et al.* Outcome of alveolar hemorrhage in hematopoietic stem cell transplant recipients. *Bone Marrow Transplant* 2007; **40**: 71–78.
27 Elsner HA, Duhrsen U, Hollwitz B, Kaulfers PM, Hossfeld DK. Fatal pulmonary hemorrhage in patients with acute leukemia and fulminant pneumonia caused by *Stenotrophomonas maltophilia*. *Ann Hematol* 1997; **74**: 155–161.
28 Rousseau A, Morcos M, Amrouche L, Foïs E, Casetta A, Rio B *et al.* Lethal pulmonary hemorrhage caused by a fulminant Stenotrophomonas maltophilia respiratory infection in an acute myeloid leukemia patient. *Leuk Lymphoma* 2004; **45**: 1293–1296.
29 Ortin X, Jaen-Martinez J, Rodriguez-Luaces M, Alvaro T, Font L. Fatal pulmonary hemorrhage in a patient with myelodysplastic syndrome and fulminant pneumonia caused by *Stenotrophomonas maltophilia*. *Infection* 2007; **35**: 201–202.
30 Takahashi N, Yoshioka T, Kameoka Y, Tagawa H, Fujishima N, Saitoh H *et al.* Fatal hemorrhagic pneumonia caused by Stenotrophomanas maltophilia in a patient with non-Hodgkin lymphoma. *J Infect Chemother* 2011; **17**: 858–862.
31 O'Brien M, Davis GH. Enzymatic profile of *Pseudomonas maltophilia*. *J Clin Microbiol* 1982; **16**: 417–421.
32 Windhorst S, Frank E, Georgieva DN, Genov N, Buck F, Borowski P *et al.* The major extracellular protease of the nosocomial pathogen *Stenotrophomonas maltophilia*: characterization of the protein and molecular cloning of the gene. *J Biol Chem* 2002; **277**: 11042–11049.

Immunology Letters 144 (2012) 33–40

Contents lists available at SciVerse ScienceDirect

Immunology Letters

journal homepage: www.elsevier.com/locate/immlet

Real-time *in vivo* cellular imaging of graft-*versus*-host disease and its reaction to immunomodulatory reagents

Takahiro Yamazaki[a], Kazunori Aoki[a], Yuji Heike[b], Sung-Won Kim[b], Takahiro Ochiya[c], Takako Wakeda[b], Robert M. Hoffman[d,e], Yoichi Takaue[b,g], Hitoshi Nakagama[f], Yoshinori Ikarashi[a,h,*]

[a] *Division of Gene and Immune Medicine, National Cancer Center Research Institute, 5-1-1, Tsukiji, Chuo-ku, Tokyo 104-0045, Japan*
[b] *Department of Hematology and Hematopoietic Stem Cell Transplantation, National Cancer Center Hospital, Japan*
[c] *Division of Molecular and Cellular Medicine, National Cancer Center Research Institute, Japan*
[d] *AntiCancer, Inc., 7917 Ostrow Street, San Diego, CA 92111, United States*
[e] *Department of Surgery, University of California San Diego, 200 West Arbor Drive, San Diego, CA 92103-8220, United States*
[f] *Division of Cancer Development System, National Cancer Center Research Institute, Japan*
[g] *Institute for Research, St. Luke's International Hospital, Akashi-cho, Chuo-ku, Tokyo104-8560, Japan*
[h] *Central Animal Division, National Cancer Center Research Institute, Japan*

ARTICLE INFO

Article history:
Received 28 December 2011
Received in revised form 2 March 2012
Accepted 4 March 2012
Available online 15 March 2012

Keywords:
In vivo cellular imaging
GFP
Allogeneic hematopoietic stem cell transplantation
Graft-*versus*-host disease
Immunomoduratory drug

ABSTRACT

Visualizing the *in vivo* dynamics of individual donor cells after allogeneic hematopoietic stem cell transplantation (HSCT) will enable deeper understanding of the process of graft-*versus*-host disease (GVHD) and graft-*versus*-leukemia (GVL). In this study, using non-invasive *in vivo* fluorescence imaging of the ear pinna, we successfully visualized green fluorescent protein (GFP) donor cells at the single cell level in the skin. This imaging model enabled visualization of the movement of GFP cells into blood vessels in real time after allogeneic HSCT. At day 1, a few donor cells were detected, and the movement of donor cells in blood vessels was readily observed at day 4. Early donor cell infiltration into non-lymphoid tissue was increased by treatment with croton oil, as an inflammatory reagent. Treatment with dexamethasone, as an anti-inflammatory reagent, suppressed donor cell infiltration. The *in vivo* cellular fluorescence imaging model described here is a very useful tool for monitoring individual donor cells in real-time and for exploring immunomodulatory reagents for allogeneic HSCT, as well as for understanding the mechanism of GVHD.

1. Introduction

Allogeneic hematopoietic stem cell transplantation (HSCT) is an effective cell-therapy for hematological malignancies [1–3]. Donor immune cells in the graft promote the elimination of leukemic cells known as graft-*versus*-leukemia (GVL). However, donor T cells, which recognize major and minor histocompatibility antigenic disparity between donor and host, trigger host-tissue damage, termed graft-*versus*-host disease (GVHD), which is a potentially fatal adverse reaction of allogeneic HSCT [2–5]. The control of GVHD is one of the major challenges in clinical oncology. *In vivo* imaging techniques using green fluorescent protein (GFP) or luciferase transgenic mice as donors have been used to visualize the dynamics of donor immune cells after allogeneic HSCT. Imaging has demonstrated that donor T cells initially migrate into secondary lymphoid tissues where they undergo activation and proliferation and enter target tissues, such as the liver, gastrointestinal tract and skin [6–11].

In vivo fluorescence imaging has been widely used for whole-body visualization in real time and multiple colors [12–20]. Further, single cell imaging can visualize lymphocyte trafficking in lymphatic and blood vessels [21,22], as well as cell-to-cell interaction in lymph nodes [23,24]. In a GVHD mouse model, donor cells were tracked at the single-cell level *in vivo* [7,25].

In this study, using *in vivo* fluorescence imaging with cellular resolution, we evaluated the effects of immunomodulatory drugs on donor-cell migration at the single-cell level in non-lymphoid tissue such as ear pinna. It was thus possible to assess the effects of the drug, and have a control, in the same animal when the drug was painted on one ear pinna with the other serving as a control.

2. Materials and methods

2.1. Mice

Female C57BL/6-Tg (CAG-EGFP) mice (termed B6-GFP-Tg, H-$2^{b/b}$), ubiquitously expressing enhanced green fluorescence protein [26], and (C57BL/6NCrSlc × DBA/2CrSlc) F_1 (termed BDF1, H-$2^{b/d}$)

* Corresponding author at: Central Animal Division, National Cancer Center Research Institute, 5-1-1, Tsukiji, Chuo-ku, Tokyo 104-0045, Japan.
Tel.: +81 3452 2511x4452; fax: +81 3248 1631.
E-mail addresses: yikarash@gan2.ncc.go.jp, yikarash@ncc.go.jp (Y. Ikarashi).

0165-2478/$ – see front matter © 2012 Elsevier B.V. All rights reserved.
doi:10.1016/j.imlet.2012.03.004

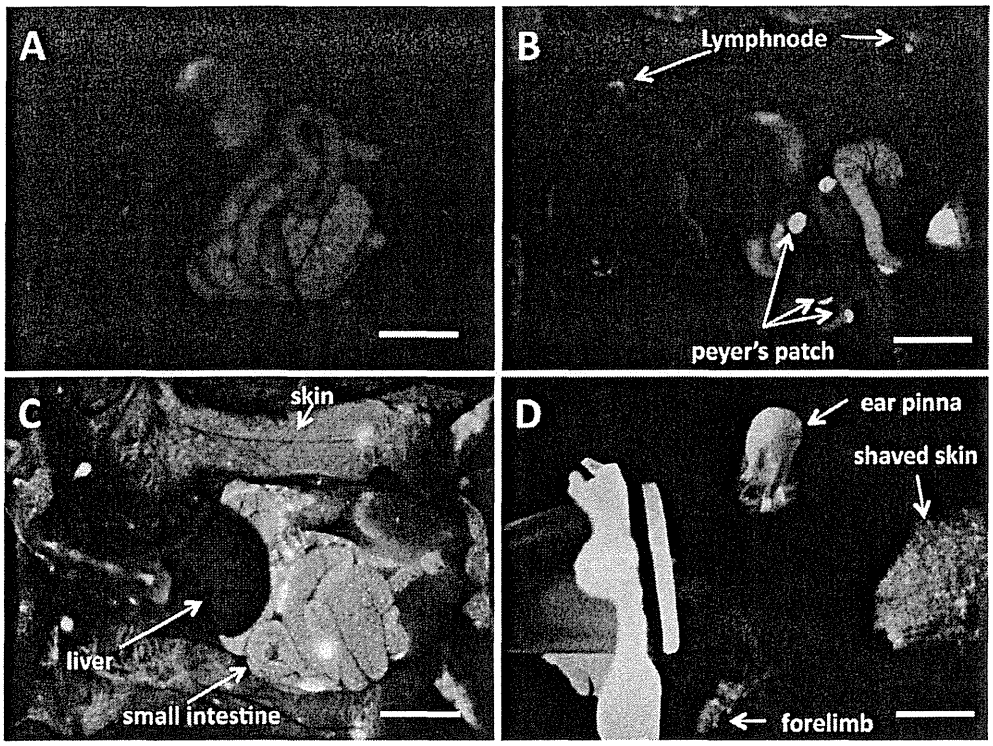

Fig. 1. *In vivo* fluorescence imaging of donor cells in opened mice after allogeneic HSCT. Spleen and bone marrow cells from B6-GFP-Tg donor mice were injected intravenously into BDF1 mice. (A–C) Mice were sacrificed and opened. GFP donor cells in whole body were visualized with the OV110 Small Animal Imaging System (A: control, B: 1 day, C: 14 days). (D) Thirty five days after transplantation, shaved mice were anesthetized and imaged with the OV110. Arrows indicate GFP+ cells in organs.

mice, were purchased from Japan SLC, Inc. (Hamamatsu, Japan). All mice were maintained in specific pathogen-free conditioned animal facilities at the National Cancer Center Research Institute. Mice between 8 and 12 weeks of age were used for all transplantation experiments. Animal studies were carried out according to the Guideline for Animal Experiments and approved by the committee for ethics of animal experimentation at the National Cancer Center.

2.2. Allogeneic HSCT mice model and treatment with immunomoduratory reagents

A mixture of 5×10^7 spleen cells and 5×10^6 bone marrow cells from B6-GFP-Tg mice was injected intravenously *via* the tail vein into untreated BDF1 mice as described previously [27,28]. Croton oil, used as an inflammatory regent, and dexamethasone, used as an anti-inflammatory reagent, were obtained from Sigma–Aldrich (St. Louis, MO). At 3 h or 7 days after allogeneic HSCT, the mice were painted on the right ear pinna with croton oil (acetone 1 μl/20 μl) or dexamethasone (acetone 0.5 μg/20 μl), respectively. As a control, the same mice were painted on the left ear pinna with 20 μl acetone alone.

2.3. Variable magnification in vivo fluorescence imaging

The OV110 Small Animal Imaging System (Olympus, Tokyo, Japan) with a cooled charge-coupled device CCD color camera and a GFP-bandpass filter, was used for non-invasive imaging from macro to micro [13]. The mice were anesthetized with isoflurane by inhalation, and sequentially imaged for the GFP donor cells in the ear pinna and shaved skin. Exposure times were optimized and identical for each experiment. Video was acquired at 10 frames/s. All images and video were obtained with OV110 software. To assess the effects of drugs on donor cell infiltration after allogeneic HSCT, GFP donor cell infiltration in the ear pinna was quantitatively analyzed. GFP donor cells in the ear pinna were initially counted and calculated as the number of donor cells per mm^2. At later stages after transplantation, the fluorescence intensity of GFP was calculated with OV110 software. To avoid contamination of autofluorescence from hair, images were obtained from the hairless areas in the ear pinna. When video of the movement of GFP cells in the blood vessels was made, hair in the ear pinna was removed by epilation to avoid autofluorescence.

2.4. Donor cell imaging in tissue sections and immunofluorescence staining

Tissues were fixed with 4% paraformaldehyde in PBS at 4 °C for 1 h followed by transfer into 10% sucrose in PBS for 12–24 h and 20% sucrose in PBS over 12 h. The tissues were embedded into an O.C.T. compound (Miles Laboratory, IN), and quickly frozen in cold isopentane. For immunofluorescence staining, the frozen block was cut into 5 μm thick sections with a cryostat (Sakura Finetek Japan, Tokyo, Japan). The sections were air-dried and incubated with blocking solution (5% normal goat serum and 1% bovine serum albumin in PBS) for 30 min and then incubated overnight at 4 °C with anti-CD3ε (500A2, eBioscience, San Diego, CA). Sections were then incubated with Alexa Fluor 594-conjugated goat anti-rat IgG antibody (invitrogen) for 1 h at room temperature. After each incubation, sections were washed with PBS containing 0.01% Triton X. Sections were mounted with VECTASHIELD with DAPI

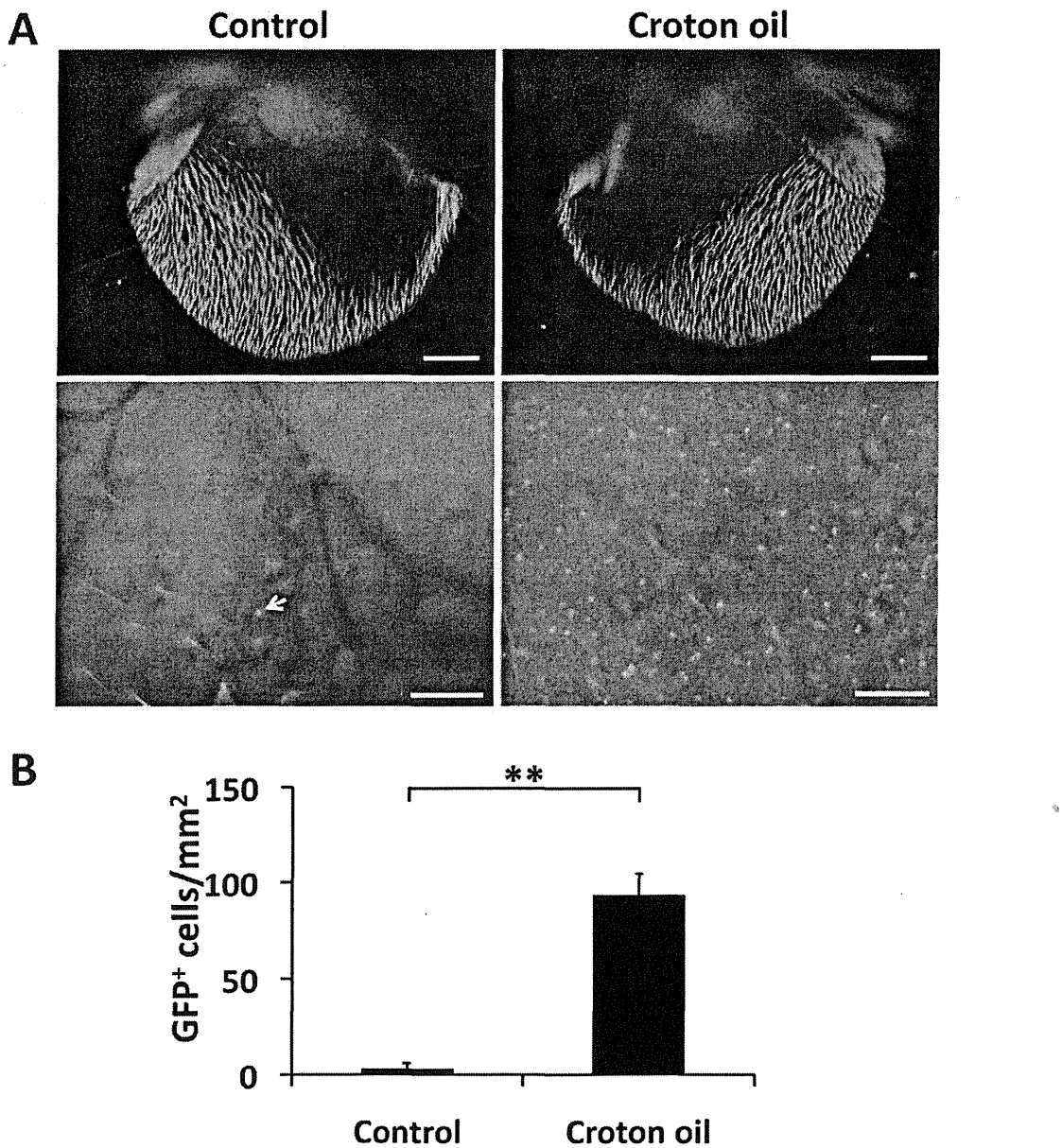

Fig. 2. Quantitative *in vivo* fluorescence imaging of donor cells in the ear pinna and the effects of inflammatory agents. (A) At 3 h after transplantation, croton oil (right panels) and acetone alone as a control (left panels), were painted on right and left ears, respectively. At day 1, GFP donor cells in the ear pinna were imaged. Low magnification images are in upper panels (scale bar, 2 mm) and high magnification images are in lower panels (scale bar, 250 μm.). Data are representative of 7 mice. (B) At day 1 after transplantation, GFP cells were counted in the ear pinna with high magnification and the number of GFP cells per 1 mm^2 was calculated. The data were from 13 fields from 5 mice and show mean ± SD. $^{**}p < 0.01$. Arrow indicates GFP+ cell.

(Vector Laboratories, Inc., Burlingame, CA). The sections were observed under fluorescence microscopy (Eclipse E1000, Nikon, Tokyo, Japan) equipped with a QICAM FAST1394 CCD camera (QImage, Surrey, BC, Canada) and Meta Morph software (Universal Imaging Corp., Buckinghamshire, UK). In the tissue sections, the number of donor cells was quantitated by manually counting GFP cells.

2.5. Statistical analysis

The statistical significance of differences between experimental groups was determined using the Student's *t*-test.

3. Results

3.1. Fluorescence imaging of donor cells after allogeneic HSCT

Using a fluorescence macro–microscopic imaging system (OV110), we could clearly visualize GFP donor cell localization in mice with open abdomens (Fig. 1A–C). GFP fluorescence was easily distinguished from orange autofluorescence in the gastrointestinal tract (Fig. 1). Similar to previous reports [7], donor cells immediately localized to secondary lymphoid tissues and then infiltrated into the whole body in the allogeneic HSCT recipients. We readily detected GFP cells in the shaved skin, ear pinna and forelimb at day 35 after transplantation (Fig. 1D). GFP donor cells were also

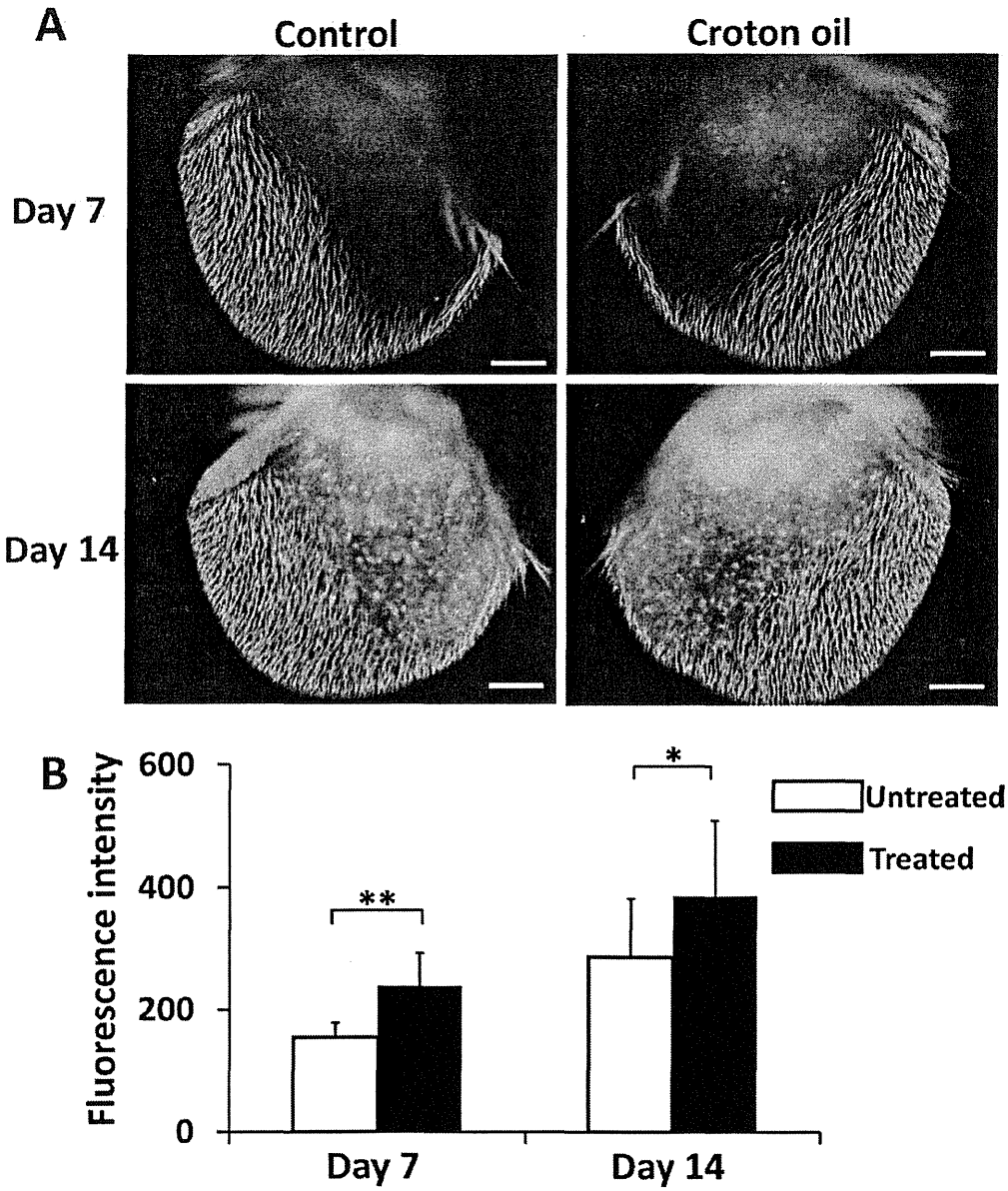

Fig. 3. *In vivo* imaging of exacerbation of donor cell infiltration by treatment with croton oil. (A) At 3 h after transplantation, croton oil (right panels) and acetone alone as control (left panels) were painted on right and left ears, respectively. At 7 (upper panels) and 14 (lower panels) days after transplantation, GFP donor cells in the ear pinna were imaged with the OV110 (scale bar, 2 mm.). Data are representative of 8–12 mice. (B) Fluorescence intensity of GFP was measured with the OV110 software. The data were from 8 mice and show mean ± SD. $^{*}p < 0.05$, $^{**}p < 0.01$.

detected in the liver, small intestine, lymphnode and Peyer's patch at the single-cell level in the dissected mice (data not shown).

3.2. *Non-invasive in vivo fluorescence imaging of donor cells in the ear pinna at the single-cell level after allogeneic HSCT*

To sequentially monitor donor cell infiltration after transplantation in the same mouse, we imaged the donor cells in the ear pinna. We determined whether donor cells could be non-invasively imaged in the ear pinna at the single-cell level. At day 1 after transplantation, donor cells were detectable at that site (Fig. 2A, lower left panel). Further, we could observe the movement of GFP donor cells into the blood vessels in the ear pinna. At day 4, GFP donor cells rapidly flowing, rolling or attaching to the vessels in the ear pinna were observed (supplemental video 1). These results indicate that it is possible to non-invasively monitor the dynamics of donor cells in the skin at the single-cell level.

3.3. *Imaging the efficacy of immunomodulatory agents*

We assessed whether non-invasive *in vivo* fluorescence imaging would be useful for screening immunomodulatory drugs for GVHD in the skin, which is a major target for GVHD. First, we tested the effect of croton oil as an inflammation stimulator after allogeneic HSCT. At 3 h after transplantation, the mice were painted with croton oil on the right ear with the left ear serving as a control. At day 1 after transplantation, increased infiltration of donor cells was clearly observed at high magnification in the ear pinna treated with croton oil (Fig. 2A). Moreover, it was possible to count GFP cells in the field and calculate the number of

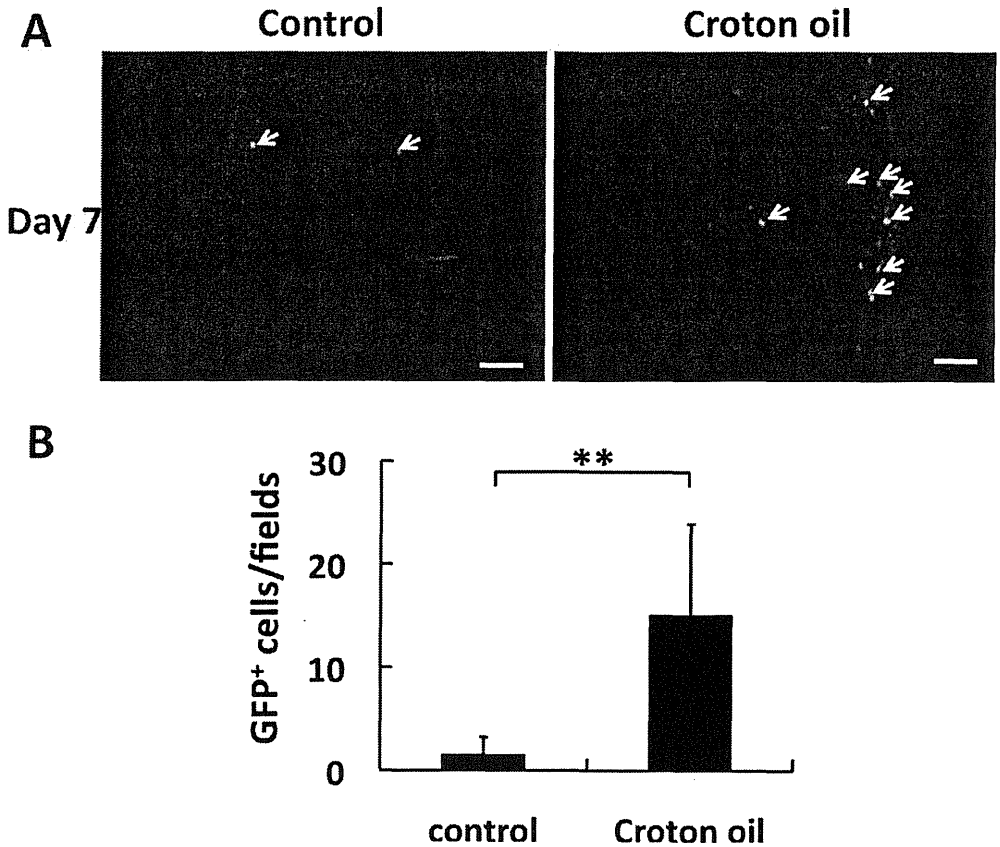

Fig. 4. Quantitative analysis of donor cell infiltration in frozen sections. (A) At 3 h after transplantation, croton oil (right panels) and acetone alone as control (left panels) were painted on right and left ears, respectively. At day 7 after transplantation, GFP cells in the frozen tissue sections were observed by fluorescence microscopy (scale bar, 50 μm.). (B) At day 7 after transplantation, GFP cells were counted in the frozen sections. Data were from 20 fields from 3 mice and show mean ± SD. $^{**}p < 0.01$.

donor cells per area. At day 1, a few GFP cells were observed in the control ear pinna, whereas approximately 90 GFP cells per mm^2 pinna accumulated in the ear after treatment with croton oil (Fig. 2B).

At 7 and 14 days after transplantation, donor cell infiltration was obviously increased in the ear pinna by treatment with croton oil (Fig. 3A). Since counting the number of infiltrating donor cells with the OV110 was difficult, due to the accumulation of many donor cells in the ear pinna, we calculated the fluorescence intensity per area using OV110 software. The analysis showed that donor cell infiltration was significantly increased in croton-oil-treated ear pinna at 7 and 14 days after transplantation (Fig. 3B). To validate the quantification of donor cell infiltration using *in vivo* imaging, we compared it with the conventional method of counting the number of GFP cells in frozen sections. Similar to *in vivo* imaging, GFP cells were found to be significantly increased in the frozen sections from croton-oil-treated tissue (Fig. 4). These results indicated that non-invasive *in vivo* fluorescence imaging is able to evaluate the effects of immunomodulatory drugs on donor-cell infiltration after allogeneic HSCT.

In order to determine whether anti-inflammatory drugs suppress donor-cell infiltration in allogeneic HSCT recipients, dexamethasone, as an anti-inflammatory drug, was painted on the right ear at day 7 after transplantation and monitored for alteration of donor cell infiltration (Fig. 5A). *In vivo* fluorescence imaging revealed that dexamethasone could significantly suppress donor cell infiltration at 14 days after transplantation (Fig. 5).

3.4. Identification of infiltrating cell subsets using immunofluorescence staining

Next, we identified the subsets of infiltrating cells. At day 7 after transplantation, $CD3^+$ and GFP cells were observed in the croton oil-treated ear pinna, using immunofluorescence staining (Fig. 6A and B). At day 14, dexamethasone treatment suppressed GFP-cell and $CD3^+$-cell infiltration in the skin (Fig. 6C and D). GFP^- $CD3^+$-cells derived from the host were also observed (Fig. 6B and C).

4. Discussion

An analysis of the *in vivo* dynamics of donor cells is useful for understanding the process of allogeneic HSCT, such as GVHD, GVL and reconstitution of hematopoietic and immune systems. *In vivo* imaging techniques are suitable for an analysis of the dynamics of donor cells after allogeneic HSCT and have revealed their migration and expansion patterns [6–11]. In the present report, we showed that a non-invasive *in vivo* macro–micro fluorescence imaging system is a very useful tool for monitoring donor cells at the single cell level and in real time, and for exploring inhibitory drugs and exacerbating factors of GVHD.

The skin is a major target tissue of GVHD and cutaneous involvement is the most frequent GVHD manifestation [4,5]. To monitor the skin after induction of GVHD, it was possible to non-invasively and sequentially visualize individual GFP donor cells in mice [3]. Further, using the ear pinna, GFP donor cells infiltrating the immunomodulatory drug-treated ear were able to be compared

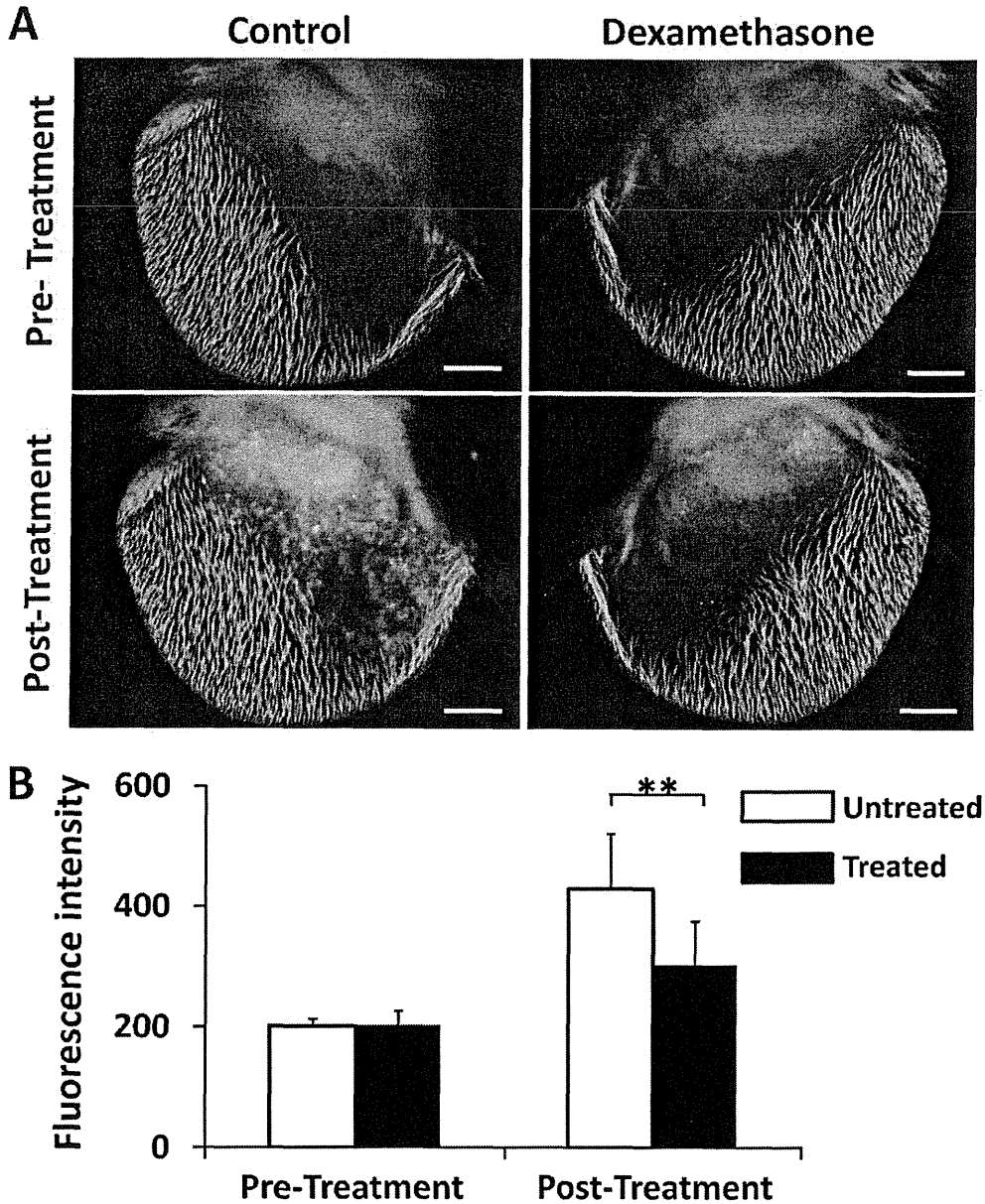

Fig. 5. The effect of dexamethasone on donor cell infiltration. (A) At 7 days after transplantation, dexamethasone (right panels) and acetone alone as control (left panels) were painted on right and left ears, respectively. Before treatment (upper panels) and at day 14 after transplantation (lower panels), GFP donor cells in the ear pinna were imaged with the OV110 (scale bar, 2 mm.). Data are representative of 8 mice. (B) Fluorescence intensity of GFP was measured with the OV110 software. The data were from 7 mice and show mean ± SD. $^{**}p < 0.01$.

with those in the untreated ear in the same animal, enabling the determination of the effects of immunomodulatory drugs for skin GVHD at the local level. It has been previously reported that donor cells could be detected in lymph nodes at 6 h [7,29]. Using fluorescence macro-microscopy, we could image individual GFP donor cells in whole ear pinna including the trafficking of donor cells in the blood vessels.

Fluorescence imaging as well as conventional methods for counting GFP cells in frozen sections revealed that GFP cell infiltration was significantly increased by croton oil. The advantages of *in vivo* fluorescence imaging are its ability to count individual GFP cells in the large area of the ear pinna and evaluate the degree of donor cell infiltration in real-time without having to make frozen sections. Moreover, we could sequentially monitor GFP cells in the same animal to compare treated and untreated ear pinna in the same mouse to evaluate the effects of drugs on skin GVHD in real time.

Regarding selectivity of donor cells recruitment, Panoskaltsis-Mortari et al. [7] reported that donor cells were observed in lymphoid tissues at 7 days after transplantation in syngeneic mice, but they are not present or present only at low levels in target tissues such as skin, liver and lung compared with allogeneic mice. Therefore, we suggest that donor cells which are observed in the skin in our report are selectively recruited.

Immunofluorescence staining analysis enabled identification of the infiltrating donor and host cell subsets in the lesions and increased our understanding of the pathogenesis of GVHD. Immunofluorescence staining revealed that at day 1 after transplantation, GFP cells detected in the ear pinna treated with croton oil were $Gr1^+$ cells, and that a large number of recipient $Gr1^+$ cells

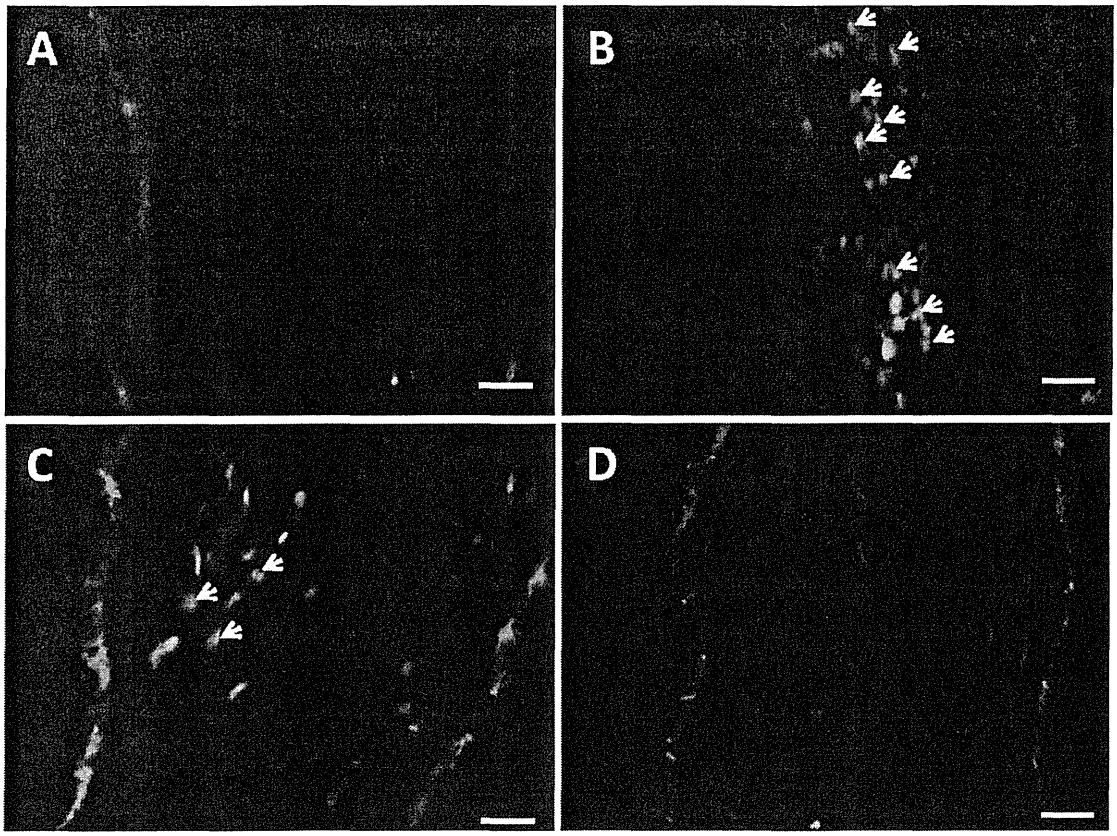

Fig. 6. Identification of infiltrating donor cell subsets using immunofluorescence staining. (A and B) At 3 h after transplantation, croton oil (B) and acetone alone as control (A) were painted on right and left ears, respectively and analyzed at day 7 after transplantation. (C and D) At day 7 after transplantation, dexamethasone (D) and acetone alone as control (C) were painted on right and left ears, respectively and analyzed at day 14 after transplantation. (A–D) Frozen sections of ear pinna were stained with CD3 monoclonal antibody and GFP and $CD3^+$ cells were observed by fluorescence microscopy (scale bar, 100 μm). Arrows indicate GFP $CD3^+$ cells (donor T cells). Data are representative of 3 mice.

(GFP^- cells) also infiltrated (data not shown). Croton oil stimulation is known to induce neutrophil accumulation [30,31]; therefore early recruitment of both donor- and recipient-type $Gr1^+$ cells could be elicited by croton oil stimulation rather than allogeneic responses. Activated neutrophils produce several chemkines such as CXCL9, CXCL10 and CXCL11 which attract CXCR3-expressing T cells [32–34]. Furthermore, on day 3 after transplantation, CXCL10 and CXCL11 produced in target tissues, directed the early recruitment of activated CXCR3-expressing donor T cells [35]. Our results showed that increased donor cell infiltration was observed in the ear pinna treated with croton oil after transplantation. We suggest that increased donor cell infiltration could be dependent not only on inflammatory responses by croton oil, but on allogeneic responses as well. Immunofluorescence staining of CD3, infiltrating T cells showed they were both donor and recipient. In this study, we used non-myeloablative allogeneic HSCT mouse models. Recipient immune cells were not depleted by conditioning; thus, recipient T cells might be involved in the lesions [22]. Treatment with corticosteroid alleviates skin GVHD, which was demonstrated by fluorescence imaging in real time.

In conclusion, non-invasive and single cell *in vivo* imaging using a fluorescence macro–microscope is very useful for drug screening for early- and late-stage GVHD in real time.

Acknowledgments

This work was supported in part by a Grant-in-Aid for scientific research from the Japan Society for the Promotion of Science, National Cancer Center Research and Development Fund, a Grant-in-Aid from the Suzuken Memorial Foundation and a Grant-in-Aid from the Advanced Clinical Research Organization.

Appendix A. Supplementary data

Supplementary data associated with this article can be found, in the online version, at doi:10.1016/j.imlet.2012.03.004.

References

[1] Horowitz MM, Gale RP, Sondel PM, Goldman JM, Kersey J, Kolb HJ, et al. Graft-versus-leukemia reactions after bone marrow transplantation. Blood 1990;75:555–62.
[2] Appelbaum FR. Haematopoietic cell transplantation as immunotherapy. Nature 2001;411:385–9.
[3] Welniak LA, Blazar BR, Murphy WJ. Immunobiology of allogeneic hematopoietic stem cell transplantation. Annu Rev Immunol 2007;25:139–70.
[4] Ferrara JL, Levine JE, Reddy P, Holler E. Graft-versus-host disease. Lancet 2009;373:1550–61.
[5] Shlomchik WD. Graft-versus-host disease. Nat Rev Immunol 2007;7:340–52.
[6] Negrin RS, Contag CH. In vivo imaging using bioluminescence: a tool for probing graft-versus-host disease. Nat Rev Immunol 2006;6:484–90.
[7] Panoskaltsis-Mortari A, Price A, Hermanson JR, Taras E, Lees C, Serody JS, et al. In vivo imaging of graft-versus-host-disease in mice. Blood 2004;103:3590–8.
[8] Stelljes M, Hermann S, Albring J, Köhler G, Löffler M, Franzius C, et al. Clinical molecular imaging in intestinal graft-versus-host disease: mapping of disease activity, prediction, and monitoring of treatment efficiency by positron emission tomography. Blood 2008;111:2909–18.
[9] Taylor PA, Ehrhardt MJ, Lees CJ, Panoskaltsis-Mortari A, Krieg AM, Sharpe AH, et al. TLR agonists regulate alloresponses and uncover a critical role for donor APCs in allogeneic bone marrow rejection. Blood 2008;112:3508–16.

[10] Beilhack A, Schulz S, Baker J, Beilhack GF, Wieland CB, Herman EI, et al. In vivo analyses of early events in acute graft-versus-host disease reveal sequential infiltration of T-cell subsets. Blood 2005;106:1113–22.
[11] Nguyen VH, Zeiser R, Dasilva DL, Chang DS, Beilhack A, Contag CH, et al. In vivo dynamics of regulatory T-cell trafficking and survival predict effective strategies to control graft-versus-host disease following allogeneic transplantation. Blood 2007;109:2649–56.
[12] Hoffman RM. The multiple uses of fluorescent proteins to visualize cancer in vivo. Nat Rev Cancer 2005;5:796–806.
[13] Yamauchi K, Yang M, Jiang P, Xu M, Yamamoto N, Tsuchiya H, et al. Development of real-time subcellular dynamic multicolor imaging of cancer-cell trafficking in live mice with a variable-magnification whole-mouse imaging system. Cancer Res 2006;66:4208–14.
[14] Hoffman RM, Yang M. Whole-body imaging with fluorescent proteins. Nat Protoc 2006;1:1429–38.
[15] Yamauchi K, Yang M, Jiang P, Yamamoto N, Xu M, Amoh Y, et al. Real-time in vivo dual-color imaging of intracapillary cancer cell and nucleus desformation and migration. Cancer Res 2005;65:4246–52.
[16] Hoffman RM. In vivo real-time imaging of nuclear-cytoplasmic dynamics of dormancy, proliferation and death of cancer cells. APMIS 2008;116:716–29.
[17] Yamauchi K, Yang M, Hayashi K, Jiang P, Yamamoto N, Tsuchiya H, et al. Induction of cancer metastasis by cyclophosphamide pretreatment of host mice: an opposite effect of chemotherapy. Cancer Res 2008;68:516–20.
[18] Yang M, Li L, Jiang P, Moossa AR, Penman S, Hoffman RM. Dual-color fluorescence imaging distinguishes tumor cells from induced host angiogenic vessels and stromal cells. Proc Natl Acad Sci U S A 2003;100:14259–62.
[19] Yang M, Reynoso J, Jiang P, Li L, Moossa AR, Hoffman RM. Transgenic nude mouse with ubiquitous green fluorescent protein expression as a host for human tumors. Cancer Res 2004;64:8651–6.
[20] Hasegawa A, Hayashi K, Kishimoto H, Yang M, Tofukuji S, Suzuki K, et al. Color-coded real-time cellular imaging of lung T-lymphocyte accumulation and focus formation in a mouse asthma model. J Allergy Clin Immunol 2010;125:461–8.
[21] Miller MJ, Wei SH, Cahalan MD, Parker I. Autonomous T cell trafficking examined in vivo with intravital two-photon microscopy. Proc Natl Acad Sci U S A 2003;100:2604–9.
[22] Mempel TR, Scimone ML, Mora JR, von Andrian UH. In vivo imaging of leukocyte trafficking in blood vessels and tissues. Curr Opin Immunol 2004;16:406–17.
[23] Stoll S, Delon J, Brotz TM, Germain RN. Dynamic imaging of T cell-dendritic cell interaction in lymph nodes. Science 2002;296:1873–6.
[24] Mempel TR, Henrickson SE, Von Andrian UH. T-cell priming by dendritic cells in lymph nodes occurs in three distinct phases. Nature 2004;427:154–9.
[25] Chakraverty R, Côté D, Buchli J, Cotter P, Hsu R, Zhao G, et al. An inflammatory checkpoint regulates recruitment of graft-versus-host reactive T cells to peripheral tissues. J Exp Med 2006;203:2021–31.
[26] Okabe M, Ikawa M, Kominami K, Nakanishi T, Nishimune Y. 'Green mice' as a source of ubiquitous green cells. FEBS Lett 1997;407:313–9.
[27] Ikarashi Y, Matsumoto Y, Omata S, Fujiwara M. Recipient-derived T cells participate in autoimmune-like hepatic lesions induced by graft-versus-host reaction. Autoimmunity 1995;20:121–7.
[28] Kuwatani M, Ikarashi Y, Iizuka A, Kawakami C, Quinn G, Heike Y, et al. Modulation of acute graft-versus-host disease and chimerism after adoptive transfer of in vitro-expanded invariant Valpha14 natural killer T cells. Immunol Lett 2006;106:82–90.
[29] Taylor PA, Ehrhardt MJ, Lees CJ, Tolar J, Weigel BJ, Panoskaltsis-Mortari A, et al. Insights into the mechanism of FTY720 and compatibility with regulatory T cells for the inhibition of graft-versus-host disease (GVHD). Blood 2007;110:3480–8.
[30] Mizgerd JP, Bullard DC, Hicks MJ, Beaudet AL, Doerschuk CM. Chronic inflammatory disease alters adhesion molecule requirements for acute neutrophil emigration in mouse skin. J Immunol 1999;162:5444–8.
[31] Komatsu N, Waki M, Sue M, Tokuda C, Kasaoka T, Nakajima M, et al. Heparanase expression in B16 melanoma cells and peripheral blood neutrophils before and after extravasation detected by novel anti-mouse heparanase monoclonal antibodies. J Immunol Methods 2008;331:82–93.
[32] Gasperini S, Marchi M, Calzetti F, Laudanna C, Vicentini L, Olsen H, et al. Gene expression and production of the monokine induced by IFN-gamma (MIG), IFN-inducible T cell alpha chemoattractant (I-TAC), and IFN-gamma-inducible protein-10 (IP-10) chemokines by human neutrophils. J Immunol 1999;162:4928–37.
[33] Molesworth-Kenyon SJ, Oakes JE, Lausch RN. A novel role for neutrophils as a source of T cell-recruiting chemokines IP-10 and Mig during the DTH response to HSV-1 antigen. J Leukoc Biol 2005;77:552–9.
[34] Seiler P, Aichele P, Bandermann S, Hauser AE, Lu B, Gerard NP, et al. Early granuloma formation after aerosol Mycobacterium tuberculosis infection is regulated by neutrophils via CXCR3-signaling chemokines. Eur J Immunol 2003;33:2676–86.
[35] Wysocki CA, Burkett SB, Panoskaltsis-Mortari A, Kirby SL, Luster AD, McKinnon K, et al. Differential roles for CCR5 expression on donor T cells during graft-versus-host disease based on pretransplant conditioning. J Immunol 2004;173:845–54.

Gene Therapy (2013) **20,** 112–118

www.nature.com/gt

SHORT COMMUNICATION

A simple detection system for adenovirus receptor expression using a telomerase-specific replication-competent adenovirus

T Sasaki[1], H Tazawa[2,3], J Hasei[1], S Osaki [1], T Kunisada[1,4], A Yoshida[1], Y Hashimoto[3], S Yano[3], R Yoshida[3], S Kagawa[3], F Uno[3], Y Urata[5], T Ozaki[1] and T Fujiwara[3]

Adenovirus serotype 5 (Ad5) is frequently used as an effective vector for induction of therapeutic transgenes in cancer gene therapy or of tumor cell lysis in oncolytic virotherapy. Ad5 can infect target cells through binding with the coxsackie and adenovirus receptor (CAR). Thus, the infectious ability of Ad5-based vectors depends on the CAR expression level in target cells. There are conventional methods to evaluate the CAR expression level in human target cells, including flow cytometry, western blotting and immunohistochemistry. Here, we show a simple system for detection and assessment of functional CAR expression in human tumor cells, using the green fluorescent protein (GFP)-expressing telomerase-specific replication-competent adenovirus OBP-401. OBP-401 infection induced detectable GFP expression in CAR-expressing tumor cells, but not in CAR-negative tumor cells, nor in CAR-positive normal fibroblasts, 24 h after infection. OBP-401-mediated GFP expression was significantly associated with CAR expression in tumor cells. OBP-401 infection detected tumor cells with low CAR expression more efficiently than conventional methods. OBP-401 also distinguished CAR-positive tumor tissues from CAR-negative tumor and normal tissues in biopsy samples. These results suggest that GFP-expressing telomerase-specific replication-competent adenovirus is a very potent diagnostic tool for assessment of functional CAR expression in tumor cells for Ad5-based antitumor therapy.

Gene Therapy (2013) **20,** 112–118; doi:10.1038/gt.2011.213; published online 12 January 2012

Keywords: oncolytic virus; adenovirus; telomerase; sarcoma; GFP

INTRODUCTION

Adenovirus serotype 5 (Ad5) is widely and frequently used as an effective vector in cancer gene therapy and oncolytic virotherapy.[1–3] Adenovirus-mediated transgene transduction is a highly efficient method for induction of ectopic transgene expression in tumor cells.[1,2] The p53 tumor suppressor gene, which is a potential therapeutic transgene that may induce a very strong antitumor effect, has been transduced into tumor cells using a replication-deficient adenovirus vector (Ad-p53, Advexin, Intorgen Therapeutics, Inc., Austin, TX, USA), and Ad-p53 has been reported to induce an antitumor effect in clinical studies.[4–7] Recently, an Ad5-based replication-competent oncolytic adenovirus has been developed as a promising anticancer reagent for induction of tumor-specific cell lysis.[8,9] Ad5-based vectors infect human target cells through binding with the coxsackie and adenovirus receptor (CAR).[10] Thus, the infection efficiency of Ad5-based vectors mainly depends on the CAR expression level in tumor tissues.[11–17] Increased CAR expression has been frequently shown in tumor cells in various organs such as the brain,[18] thyroid,[19] esophagus,[20] gastrointestinal tract,[21] prostate,[14] bone and soft tissues.[22–24] However, tumor cells often show reduced CAR expression following tumor progression.[18,21,25,26] Decreased CAR expression has also been shown in tumor tissues after repeated injection of Ad-p53.[27,28] It is therefore necessary to assess the CAR expression level of target tumor tissues before and after Ad5-based cancer gene therapy and oncolytic virotherapy.

There are some conventional methods for evaluation of the CAR expression level in tumor tissues, such as flow cytometry, immunohistochemistry, western blotting and reverse transcription (RT)-PCR. Flow cytometry is mainly used to detect CAR-positive human tumor cell lines.[13,24,28,29] Immunohistochemistry is frequently used to assess CAR expression in various human tumor tissues.[11,14,20,23,25] Western blotting is usually performed to confirm the expression of many types of proteins including CAR in molecular biological experiments. Quantitative RT-PCR is also a useful method for evaluation of the mRNA expression of CAR.[18,22] Although these conventional methods can detect CAR expression in tumor tissues, it still remains unclear whether Ad5-based vectors really infect target tumor cells through binding with the CAR that is detected using conventional methods. Therefore, the development of a novel method for assessment of the level of expression of functional CAR in tumor tissues, which is what the Ad5-based vectors really bind, is required for Ad5-based anticancer therapy.

We previously developed a telomerase-specific replication-competent adenovirus OBP-301 (Telomelysin, Oncolys BioPharma, Inc., Tokyo, Japan) that drives the *E1A* and *E1B* genes under the human telomerase reverse transcriptase (*hTERT*) promoter.[8,29–31] OBP-301 infects both normal and tumor cells that express CAR, but replicates only in CAR-positive tumor cells in a telomerase-dependent manner. Furthermore, we recently generated a green fluorescent protein (GFP)-expressing telomerase-specific replication-

[1]Department of Orthopaedic Surgery, Okayama University Graduate School of Medicine, Dentistry and Pharmaceutical Sciences, Okayama, Japan; [2]Center for Gene and Cell Therapy, Okayama University Hospital, Okayama, Japan; [3]Department of Gastroenterological Surgery, Okayama University Graduate School of Medicine, Dentistry and Pharmaceutical Sciences, Okayama, Japan; [4]Department of Medical Materials for Musculoskeletal Reconstruction, Okayama University Graduate School of Medicine, Dentistry and Pharmaceutical Sciences, Okayama, Japan and [5]Oncolys BioPharma, Inc., Tokyo, Japan. Correspondence: Professor T Fujiwara, Department of Gastroenterological Surgery, Okayama University Graduate School of Medicine, Dentistry and Pharmaceutical Sciences, 2-5-1 Shikata-cho, Kita-ku, Okayama 700-8558, Japan.
E-mail: toshi_f@md.okayama-u.ac.jp
Received 15 July 2011; revised 7 November 2011; accepted 5 December 2011; published online 12 January 2012

competent adenovirus OBP-401, which induces ectopic GFP expression in tumor cells, but not in normal cells.[32] OBP-401 infection efficiently induces GFP expression in metastatic tumor cells at regional lymph nodes[32] and liver,[33] circulating tumor cells in blood flow[34] and disseminated tumor cells in the abdominal cavity.[35] These results suggest that OBP-401 is a highly sensitive tool for the detection of tumor cells. Furthermore, Ad5-based OBP-401 would also be useful for induction of GFP expression in CAR-positive tumor cells, but not in CAR-negative tumor cells.

In the present study, we evaluated whether induction of GFP expression by OBP-401 infection is associated with CAR expression in tumor cells. OBP-401-mediated GFP induction was further examined in xenograft tumor tissues that have different levels of CAR expression and in surrounding normal tissues.

RESULTS AND DISCUSSION

Assessment of an OBP-401 infection protocol for the detection of CAR-positive tumor cells

We recently demonstrated that the level of CAR expression that was detected using flow cytometry was significantly associated with OBP-301-mediated cytopathic activity in human bone and soft tissue sarcoma cells.[29] Furthermore, OBP-401 infection has been shown to induce GFP expression 24 h after infection of human sarcoma cells.[34] To evaluate whether GFP expression that is induced by OBP-401 infection is associated with CAR expression in tumor cells, we used three human sarcoma cell lines (OST, NMFH-1 and OUMS-27) that have different levels of CAR expression, as previously reported.[29] Flow cytometric analysis confirmed that OST cells showed detectable CAR expression, whereas cells of the NMFH-1 and OUMS-27 sarcoma cell lines had no detectable CAR expression (Figure 1a).

To determine suitable conditions for OBP-401 infection in order to detect CAR-positive tumor cells, OST sarcoma cells were infected with OBP-401 at multiplicity of infections (MOIs) of 1, 10 and 100 plaque-forming units (PFU) per cell over 24 h (Figure 1b and c). Twelve hours after infection, only OBP-401 infection at an MOI of 100 had induced GFP expression in all of the OST cells. Twenty-four hours after infection, OBP-401 infection at MOIs of 10 and 100 had induced ectopic GFP expression in all of the OST cells, whereas OBP-401 infection at an MOI of 1 had induced GFP expression in about 80% of the OST cells. These results indicate that OBP-401 infection at an MOI of greater than 10 is necessary to efficiently detect CAR-positive tumor cells 24 h after infection.

To subsequently determine a suitable condition for OBP-401 infection that would exclude CAR-negative tumor cells, the NMFH-1 and OUMS-27 sarcoma cells that do not express CAR were infected with OBP-401 at MOIs of 10 and 100 for 60 h (Figures 1d and e). NMFH-1 cells expressed GFP at 24 and 48 h after OBP-401 infection at MOIs of 100 and 10, respectively. In contrast, OUMS-27 cells exhibited no GFP expression after OBP-401 infection. To investigate the different GFP expression between these CAR-negative tumor cells, expression of integrins, $\alpha v\beta 3$ and $\alpha v\beta 5$, was further examined by flow cytometry. NMFH-1 cells showed twofold higher expression of integrin $\alpha v\beta 3$ compared with OUMS-27 cells, whereas $\alpha v\beta 5$ expression was similar in these cells (Supplementary Figure S1a). These results indicate that OBP-401 infection at an MOI of 10 for 24 h is a suitable protocol for distinguishing CAR-negative tumor cells from CAR-positive tumor cells, when CAR-negative tumor cells express integrin molecules.

Relationship between OBP-401-induced GFP expression and CAR expression

To evaluate whether OBP-401-induced GFP expression correlates with CAR expression in tumor cells, six human sarcoma cell lines (OST, U2OS, NOS-10, MNNG/HOS, NMFH-1 and OUMS-27) and normal human lung fibroblasts (NHLF) cells that have different levels of CAR expression (Figure 1a and Supplementary Figure S1b) were infected with OBP-401 at an MOI of 10 for 24 h, and the GFP-positive cells in each cell type were analyzed under fluorescence microscopy (Figures 2a and b). OBP-401 infection-induced GFP expression from 12 h after infection and, after 24 h, more than 40% of all CAR-positive tumor cells (OST, U2OS, NOS-10 and MNNG/HOS) were detected as GFP-positive cells. However, no GFP-positive cells were detected in the CAR-negative tumor cells (NMFH-1, OUMS-27), or in the normal NHLF cells, 24 h after infection. Furthermore, OBP-401-mediated GFP induction in CAR-positive tumor cells was suppressed by blocking CAR proteins with anti-CAR antibody (Supplementary Figure S2). To assess the GFP expression level in all tumor and normal cells in a more quantitative manner, we quantified the level of GFP fluorescence in each cell type 24 h after infection using a fluorescence microplate reader (Figure 2c). We also quantified the level of CAR expression in these cells by calculating the mean fluorescence intensity in flow cytometric analysis (Figure 2d). GFP fluorescence was detected in CAR-positive tumor cells, but not in either CAR-negative tumor cells or in CAR-positive normal cells. There was a significant relationship between the CAR expression level and the GFP fluorescence level ($r = 0.885$; $P = 0.019$) (Figure 2e). These results indicate that OBP-401-mediated GFP expression is highly associated with CAR expression in tumor cells.

Comparison of the potential of OBP-401-mediated GFP induction and of conventional methods for CAR detection

To estimate the potential of OBP-401-mediated GFP induction for the detection of CAR-positive tumor cells, we compared the above protocol using OBP-401 with western blot analysis and immunocytochemistry. CAR expression was detected in OST, U2OS and NOS-10 sarcoma cells, but not in CAR-positive MNNG/HOS sarcoma cells, using western blot analysis (Supplementary Figure S3a). In contrast, only OST cells displayed a positive CAR signal using immunocytochemistry, whereas the CAR signal of the other three CAR-positive tumor cells was almost as weak as that from CAR-negative tumor cells (Supplementary Figure S3b). CAR expression was also not detected in CAR-positive NHLF cells by either western blot analysis or by immunocytochemistry. These results suggest that the GFP induction protocol using OBP-401 is more sensitive for the detection of CAR-positive tumor cells than conventional methods.

OBP-401-mediated GFP induction was detected in MNNG/HOS sarcoma cells that expressed a low level of CAR (Figure 2c), although neither western blot analysis nor immunocytochemistry detected CAR in these cells (Supplementary Figure S3). Furthermore, although conventional methods may be able to detect high CAR expression in tumor cells, whether the CAR expression that is detected by conventional methods is really functional for binding with Ad5-based vectors still remains unclear. In contrast, as OBP-401 is an Ad5-based vector that expresses a fluorescent *GFP* gene, OBP-401-induced GFP expression directly proves that the CAR that is expressed is functional for Ad5-based vector binding. Thus, the OBP-401-mediated GFP induction strategy is a potential diagnostic method that can efficiently and directly assess functional CAR expression in tumor cells.

OBP-401-mediated GFP induction in xenograft tumor and normal tissues with different CAR expression

Finally, to investigate the potential of the OBP-401-mediated method for the detection of CAR expression in tumor and normal tissues, we used this method to analyze CAR expression of human xenograft tumor tissues, that do or do not express CAR, as well as of surrounding normal muscle tissues, which have been previously shown to lose CAR expression.[36] CAR-positive OST sarcoma cells or CAR-negative OUMS-27 sarcoma cells were inoculated into nude

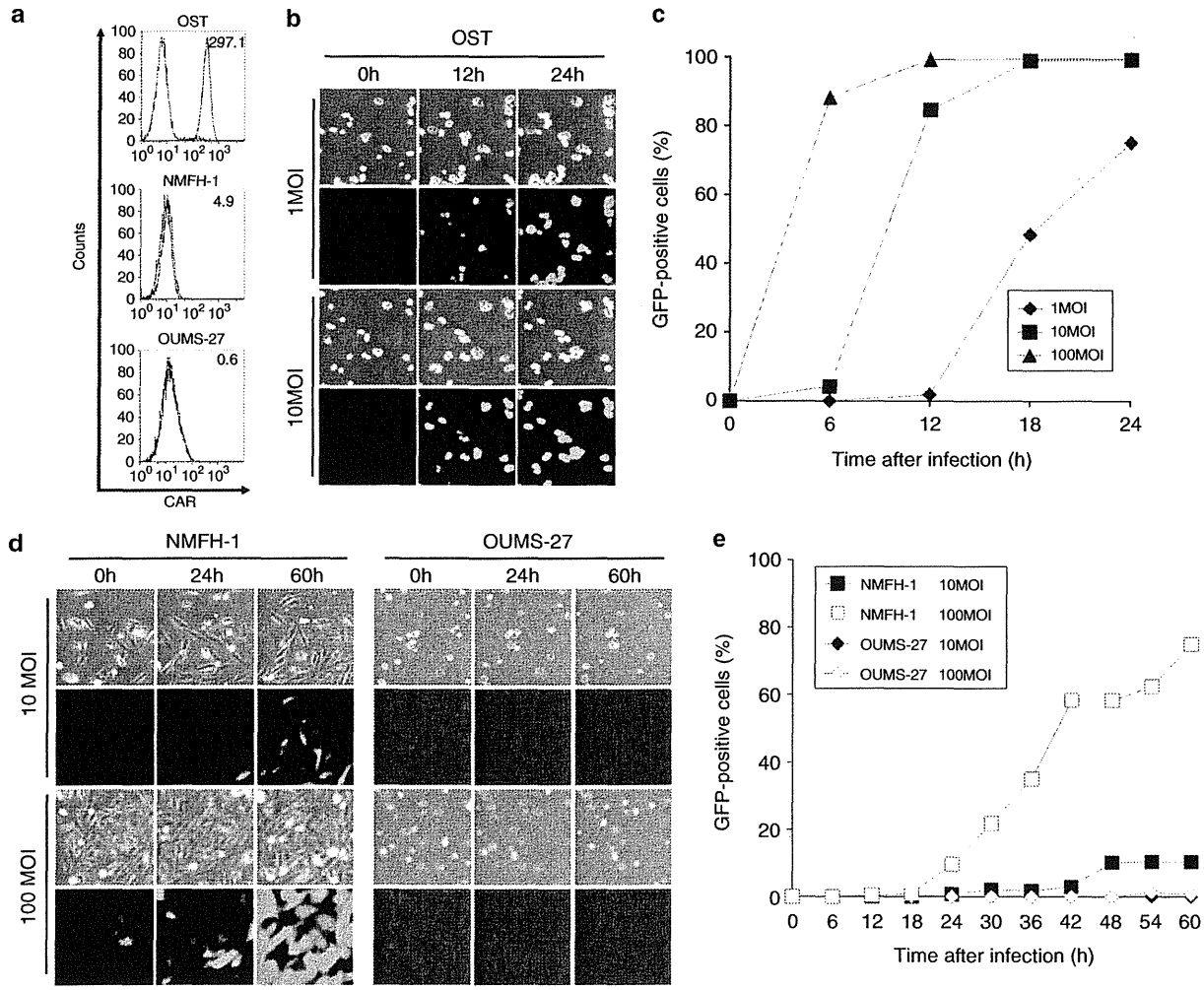

Figure 1. Establishment of a suitable protocol for the detection of CAR expression using OBP-401. (**a**) The level of CAR expression on three human sarcoma cell lines (OST, NMFH-1 and OUMS-27) was analyzed using flow cytometry. The cells were incubated with a monoclonal anti-CAR (RmcB) antibody and the signal was detected using a fluorescent isothiocyanate (FITC)-labeled secondary antibody. The mean fluorescence intensity (MFI), which is a measure of CAR and integrin expression, was calculated for each cell and is shown at the top right of each graph. (**b**) Time-lapse images of OST cells, which displayed the highest CAR expression, were recorded for 24 h after OBP-401 infection at MOIs of 1 and 10 PFU per cell. Representative images taken at the indicated time points and MOIs show cell morphology that was analyzed using phase-contrast microscopy (top panels) and GFP expression that was analyzed using fluorescence microscopy (bottom panels). Original magnification: × 80. (**c**) The percentage of GFP-positive cells was counted in OST cells at the indicated time points after OBP-301 infection at MOIs of 1, 10 and 100 PFU per cell. (**d**) Time-lapse images of non-CAR-expressing OUMS-27 and NMFH-1 cells were recorded for 60 h after OBP-401 infection at MOIs of 10 and 100 PFU per cell. Representative images taken at the indicated time points and MOIs show cell morphology that was analyzed using phase-contrast microscopy (top panels) and GFP expression that was analyzed using fluorescence microscopy (bottom panels). Original magnification: × 80. (**e**) The percentage of OUMS-27 and NMFH-1 GFP-positive cells was counted at the indicated time points after OBP-301 infection at MOIs of 10 and 100 PFU per cell.

mice to develop xenograft tumors. After resection of the OST tumors, the OUMS-27 tumors and normal muscle tissue, the tissues were subjected to the protocol for OBP-401-mediated GFP induction using a three-step procedure (Figure 3a) as follows; step 1: OBP-401 infection for 24 h, step 2: washing with PBS and step 3: observation under a fluorescence microscope. As shown in Figure 3b, OBP-401 infection-induced GFP expression in CAR-positive OST tumor tissues, but not in CAR-negative OUMS-27 tumor tissues or in normal muscle tissue. These results suggest that OBP-401-mediated GFP induction is a simple and useful method for the detection of CAR expression by tumor tissues.

Flow cytometry is a highly sensitive conventional method for the detection of cell surface CAR expression, which is associated with the therapeutic efficacy of Ad5-based vectors in tumor cells.[13,24,28,29] However, as many tumor cells tightly bind to each other or to normal stromal cells within tumor tissues, the preparation of single tumor cells is not easy, and therefore flow cytometry is an inadequate method for the detection of CAR expression in tumor tissues. In contrast, the preparation of single tumor cells is not necessary for the OBP-401-mediated GFP induction protocol. Furthermore, assay of OBP-401-induced GFP expression was more sensitive than flow cytometry (Figure 2d) in distinguishing CAR-positive normal cells from CAR-positive tumor cells (Figure 2c). Thus, the OBP-401-mediated GFP induction method is a simple and tumor-specific system for the detection of CAR expression in tumor tissues.

Fluorescent proteins including GFP have great potentials to visualize tumor cells in real time on the *in vivo* setting.[37,38]

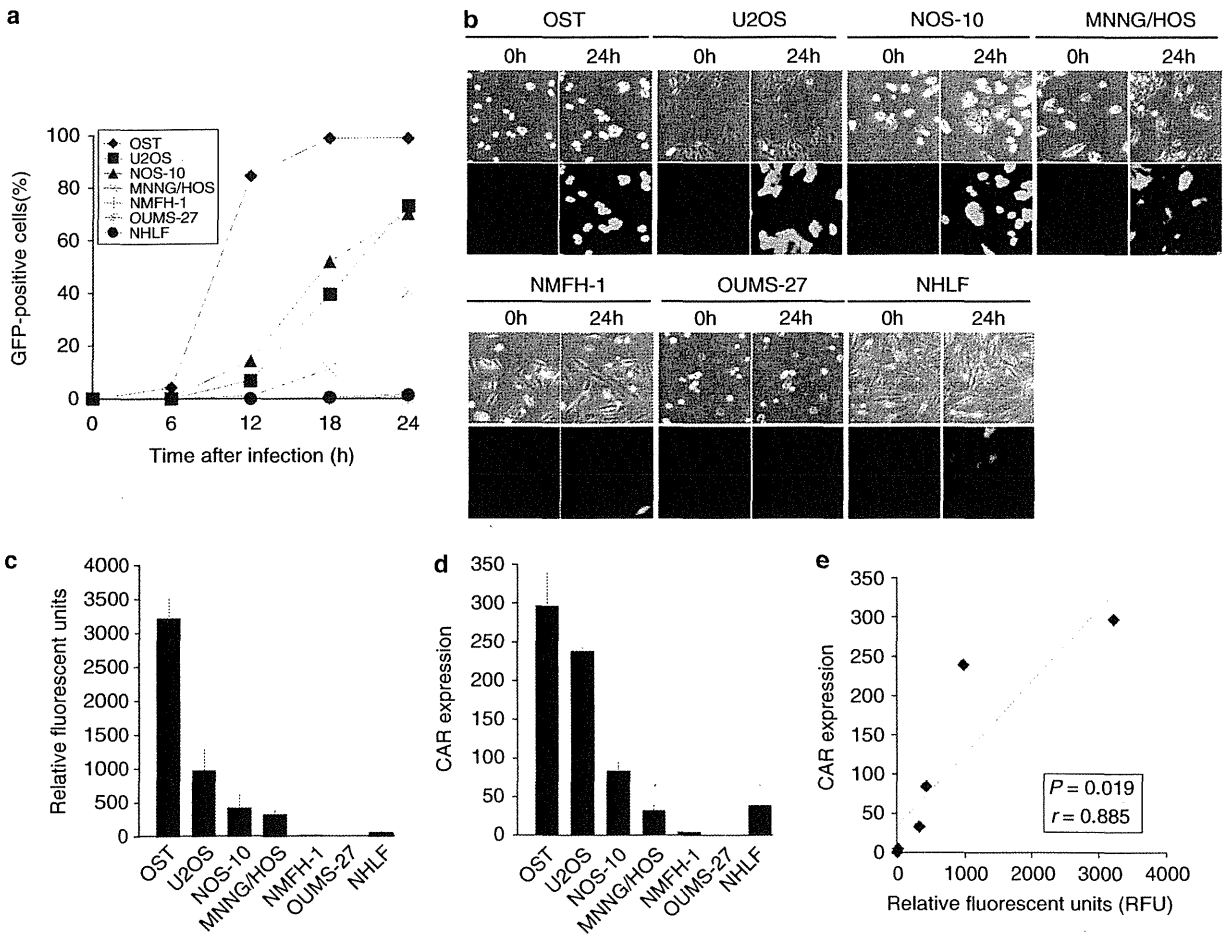

Figure 2. *In vitro* CAR-dependent GFP expression induced by OBP-401 infection. (**a**) The percentage of GFP-positive cells in all tumor and normal cells was counted at the indicated time points after OBP-301 infection at an MOI of 10 PFU per cell. (**b**) Time-lapse images of all tumor and normal cells were recorded for 24 h after infection with OBP-401 at an MOI of 10 PFU per cell. Representative images taken at the indicated time points show cell morphology that was analyzed using phase-contrast microscopy (top panels) and GFP expression that was analyzed using fluorescence microscopy (bottom panels). Original magnification: × 80. (**c**) Quantitative assessment of the level of GFP fluorescence in all tumor and normal cells 24 after OBP-401 infection at an MOI of 10 PFU per cell, using a fluorescent microplate reader with excitation/emission at 485 nm/528 nm. The intensity of GFP fluorescence was evaluated based on the brightness determinations used as relative fluorescence units (RFU). (**d**) The mean fluorescent intensity (MFI) of (CAR) expression on human sarcoma cells and normal fibroblasts. The cells were incubated with a monoclonal anti-CAR (RmcB) antibody, followed by a FITC-labeled secondary antibody, and were analyzed using flow cytometry. (**e**) Relationship between the level of GFP fluorescence and CAR expression in all tumor and normal cells after OBP-401 infection. The slope represents the inverse correlation between these two factors. Statistical significance was determined as $P<0.05$, after analysis of Pearson's correlation coefficient.

We previously reported that OBP-401 can efficiently induce GFP expression in small populations of metastatic tumor cells at various regions *in vivo*.[32-35] In this study, we further demonstrated that OBP-401-mediated GFP expression provides us the important information for detection of CAR-positive tumor cells. OBP-401 with *hTERT* gene promoter-induced GFP expression in CAR-positive tumor cells with telomerase activity, but not CAR-positive normal cells without telomerase activity (Figure 2c). There was significant relationship between the CAR expression and the GFP expression in tumor cells (Figure 2d). Among the four CAR-positive tumor cells, U2OS cells showed low GFP expression compared with high CAR expression (Figure 1a and 2c). As we recently reported that U2OS cells showed low *hTERT* mRNA expression, the low activity of *hTERT* gene promoter in tumor cells would affect OBP-401-mediated GFP expression. However, as various types of human cancer cells frequently show high telomerase activities,[39] OBP-401-mediated GFP induction system would be widely useful method to evaluate CAR expression in tumor cells.

Previous reports have suggested that *ex vivo* infection of human cancer specimens with a GFP-expressing replication-deficient adenovirus[40] or a replication-selective oncolytic adenovirus[41] is a useful method for assessment of the transduction efficacy or cytopathic activity, respectively, of Ad5-based vectors in individual tumor tissues. In this study, we confirmed that the GFP-expressing telomerase-specific oncolytic adenovirus OBP-401 is useful for detection of CAR-positive tumor tissues through induction of GFP expression (Figure 3b). Interestingly, OBP-401-infected OST tumor tissues showed heterogenous GFP expression (Figure 3b), although GFP expression was induced in all OBP-401-infected OST cells *in vitro* (Figure 2b). Our finding of heterogenous GFP expression in tumor tissues, which indicates heterogenous CAR expression, is consistent with a previously reported heterogeneity in CAR expression.[42] As several factors such as hypoxia[43] and cell cycle status[44] have been suggested to affect CAR expression in tumor cells, factors in the tumor microenvironment may be involved in the heterogenous CAR expression in tumor cells.

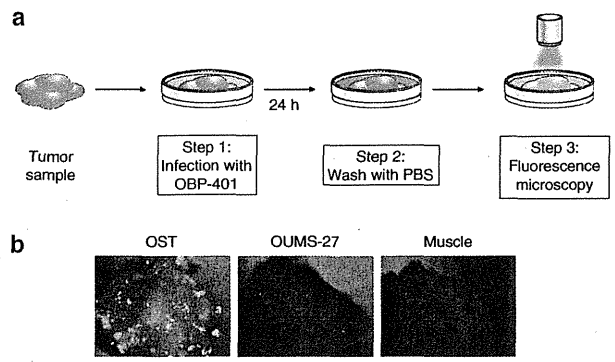

Figure 3. A simple method for detection of CAR expression in tumor tissues using OBP-401 infection. (**a**) Outline of the 3-step procedure; step 1: infection with OBP-401, step 2: washing with PBS and step 3: observation under a fluorescence microscope. Tumor tissues ($2 \times 2 \times 2\,mm^3$) were infected with OBP-401 at a concentration of 2.4×10^6 PFU for 24 h, were washed with PBS and were observed using fluorescence microscopy. (**b**) Assessment of GFP expression in the CAR-positive OST tumor (left panel), the CAR-negative OUMS-27 tumor (middle panel) and normal muscle tissues (right panel) under a fluorescence microscope. Original magnification: $\times 30$.

Furthermore, as OBP-401 induces tumor-specific GFP expression, normal stromal or epithelial cells may be involved in heterogenous GFP expression in tumor tissues.

In conclusion, we have demonstrated that the GFP-expressing telomerase-specific replication-competent adenovirus OBP-401 is a promising fluorescence imaging tool for the detection of functional and tumor-specific CAR expression in tumor tissues. OBP-401-mediated GFP induction is a simple and highly sensitive method for analysis of tumor cells compared with conventional methods. This novel CAR detection system using OBP-401 has the potential of being widely applicable to assessment of predictive biomarkers for Ad5-based vector-mediated anticancer therapy.

MATERIALS AND METHODS

Cell lines

The human osteosarcoma cell line OST was kindly provided by Dr Satoru Kyo (Kanazawa University, Ishikawa, Japan). The human osteosarcoma cell line U2OS and the transformed embryonic kidney cell line 293 were obtained from the American Type Culture Collection (ATCC; Manassas, VA, USA). The human osteosarcoma cell line NOS-10[45] and the human malignant fibrous histiocytoma cell line NMFH-1[46] were kindly provided by Dr Hiroyuki Kawashima (Niigata University, Niigata, Japan). The human osteosarcoma cell line MNNG/HOS was purchased from DS Pharma Biomedical (Osaka, Japan). The chondrosarcoma cell line OUMS-27 was previously established in our laboratory.[47] The normal human lung fibroblast cell line NHLF was obtained from TaKaRa Biomedicals (Kyoto, Japan). These cells were propagated as monolayer cultures in the medium recommended by the manufacturer. All media were supplemented with 10% heat-inactivated fetal bovine serum, 100 units ml^{-1} penicillin and 100 $\mu g\,ml^{-1}$ streptomycin. The cells were maintained at 37 °C in a humidified atmosphere containing 5% CO_2.

Recombinant adenoviruses

We previously generated and characterized OBP-401, which is a telomerase-specific replication-competent adenovirus variant, in which the *hTERT* promoter element drives the expression of *E1A* and *E1B* genes that are linked to an internal ribosome entry site, and in which the *GFP* gene is inserted into the E3 region under a cytomegalovirus promoter.[32,34] The virus was purified by ultracentrifugation using cesium chloride step gradients. Viral titers were determined by a plaque-forming assay using 293 cells and viruses were stored at −80 °C.

Flow cytometry

The cells (5×10^5 cells) were labeled with the mouse monoclonal anti-CAR (RmcB; Upstate Biotechnology, Lake Placid, NY, USA) antibody for 30 min at 4 °C. The cells were then incubated with fluorescent isothiocyanate-conjugated rabbit anti-mouse IgG second antibody (Zymed Laboratories, San Francisco, CA, USA) and were analyzed using flow cytometry (FACS Array; Becton Dickinson, Mountain View, CA, USA). The mean fluorescence intensity of CAR for each cell line was determined by calculating the differences between the mean fluorescence intensity in antibody-treated and non-treated cells in triplicate experiments.

Time-lapse confocal laser microscopy

The cells (1×10^5 cells per dish) were seeded in 35 mm glass-based dishes 20 h before virus infection. OST cells were infected with OBP-401 at an MOI of 1, 10 or 100 PFU per cell for 24 h. NMFH-1 and OUMS-27 cells were infected with OBP-401 at an MOI of 10 or 100 PFU per cell for 60 h. Other cells were infected with OBP-401 at an MOI of 10 PFU per cell for 24 h. Phase-contrast and fluorescence time-lapse recordings were obtained to concomitantly analyze cell morphology and GFP expression using an inverted FV10i confocal laser scanning microscopy (OLYMPUS; Tokyo, Japan). Photographic images were taken every 5 min. The percentage of GFP-positive cells in each field was calculated using the formula: the number of CAR-positive cells / the total number of CAR-positive and CAR-negative cells $\times 100$.

Fluorescence microplate assay

The cells (5×10^3 cells per well) were seeded on 96-well black bottomed culture plates and were incubated for 20 h before virus infection. The cells were infected with OBP-401 at an MOI of 10 for 24 h. The level of expression of GFP fluorescence was measured using a fluorescent microplate reader (DS Pharma Biomedical; Osaka, Japan) with excitation/emission at 485 nm/528 nm. The mean expression of GFP fluorescence in each cell was calculated in triplicate experiments, as previously reported.[34]

Animal experiments

Animal experimental protocols were approved by the Ethics Review Committee for Animal Experimentation of Okayama University School of Medicine. OST and OUMS-27 cells (5×10^6 cells per site) were inoculated into the flank of female athymic nude mice aged 6 to 7 weeks (Charles River Laboratories, Wilmington, MA, USA). Palpable tumors developed within 14 to 21 days and were permitted to grow to ~5 to 6 mm in diameter. At that stage, tumor and normal muscle tissues were resected. The tumor and normal tissues ($2 \times 2 \times 2\,mm^3$) were placed in 96-well plates with culture medium. As single tumor cell is about 10 μm in diameter, we considered that there are 2.4×10^5 cells on the surface area of each sample tissue. Then, we infected each sample tissue with 2.4×10^6 PFU (10 MOI per sample) of OBP-401 for 24 h. After washing with PBS, tumor and normal tissues were again placed in 96-well plates with culture medium and analyzed using an inverted fluorescence microscope (OLYMPUS).

Statistical analysis

Data are expressed as means ± s.d. Student's *t*-test was used to compare differences between groups. Pearson's product-moment correlation coefficients were calculated using PASW statistics software version 18 (SPSS Inc., Chicago, IL, USA). Statistical significance was defined as when the *P* value was less than 0.05.

ABBREVIATIONS

Ad5, Adenovirus serotype 5; CAR, coxsackie and adenovirus receptor; GFP, green fluorescent protein; RT-PCR, reverse transcription-polymerase chain reaction; hTERT, human telomerase reverse transcriptase; MOI, multiplicity of infection;